Universidade de Aveiro Departamento de Biologia
Ano 2015

MARIA JOSÉ CARDOSO LOPES

Caracterização do tecido da cicatriz glial, com foco no ácido hialurónico, após compressão medular em ratinhos.

Characterization of the glial scar tissue in a murine model of spinal cord compression, with focus on hyaluronan.

Dissertação apresentada à Universidade de Aveiro para cumprimento dos requisitos necessários à obtenção do grau de Mestre em Biologia Molecular e Celular, realizada sob a orientação científica do Doutor Charles Nicaise, principal investigador do Laboratório de Neuro degeneração e Regeneração da Faculdade de Medicina da Universidade de Namur, da Doutora Anabela Rolo, Professora auxiliar do Departamento de Ciências da Vida da Faculdade de Ciências e Tecnologias da Universidade de Coimbra e da Doutora Maria de Lourdes Gomes Pereira, Professora Associada com Agregação do Departamento de Biologia da Universidade de Aveiro.

DECLARAÇÃO

Declaro que este relatório é integralmente da minha autoria, estando devidamente referenciadas as fontes e obras consultadas, bem como identificadas de modo claro as citações dessas obras. Não contém, por isso, qualquer tipo de plágio quer de textos publicados, qualquer que seja o meio dessa publicação, incluindo meios eletrónicos, quer de trabalhos académicos.

Às pessoas da minha vida, capazes de me lerem o olhar.
À minha mãe, à minha irmã Dina e ao meu amor, Hugo.

o júri

presidente

Prof. Doutor Fernando José Mendes Gonçalves
Professor Associado com agregação do Departamento de Biologia da Universidade de Aveiro.

Prof. Doutora Helena Cristina Correia de Oliveira
Investigadora em Pós-Doutoramento do centro de estudos do ambiente e do mar (CESAM) da Universidade de Aveiro.

Prof. Doutora Maria de Lourdes Pereira
Professora Associada com agregação do Departamento de Biologia da Universidade de Aveiro.

agradecimentos

Em primeiro lugar gostaria de agradecer ao Dr. Charles Nicaise não só por me ter proporcionado a possibilidade e o privilégio de desenvolver este trabalho no seu laboratório de neurodegeneração e regeneração (LNR), mas também por todo o conhecimento transmitido e pela simpatia e amabilidade com que me recebeu, acolheu e integrou na equipa.
Obrigado pela paciência com que encarou os problemas que iam surgindo e sobretudo pela confiança depositada em mim ao longo de todos estes meses. Na sua convivência aprendi muito como pessoa e como profissional.
Obrigado também às minhas orientadoras Drª Anabela Rolo e Mª de Lourdes, pela disponibilidade demonstrada ao longo do meu trabalho.
A todos os membros do Laboratório de células e tecidos e LNR que me proporcionaram um ambiente de aprendizagem com muitos momentos de convívio e diversão durante a minha estadia.
Um obrigado à Joanna Bouchat e ao Jérémy Malaisse pelos conhecimentos transmitidos e ajuda nos cálculos de qPCR e ELISA.
Um obrigado também ao Daniel vanvlaender pelos conhecimentos práticos a nível de histologia e pelas conversas em espanhol que me levaram o pensamento para mais perto de casa.
À Valerie De Glas, à Kathleen De Swert e ao Benoit Balau pela atenção e preocupação com que sempre me atenderam e ajudaram nas questões mais práticas.
Um obrigado especial à Meryl Ribeiro pelos raros momentos em que podia desabafar e expressar-me na minha língua-mãe.
Aos meus companheiros e amigo ERASMUS: Lotta Onninen, Vesela Losanova, Kia, Marta Szukala, Victoria Esquilar, Gianvito Ostuni, Andrea Robbiani, Clara Alameda, Mónica Bertomeu, Cristi Dolce-Kourou, Pippo Len, Andrea Tugnoli, Kevin Fi, Tanguy Mazuin, Michael Bianchin, Robin Ananaba e Adeline Ht que trago no coração. Um muito obrigado pelas conversas e partilha de experiências.
Aos meus amigos Joana Monteiro, Daniela Nunes, Telma Silva, Andreia Santos e Márcio Curral pela força, motivação incansável e pela paciência durante a minha ausência.
Por último mas não menos importante, à minha família, que além de suportar a distância que este trabalho impôs, esteve sempre presente.
Obrigado pelos quilómetros percorridos na minha direção pai.
Obrigado pela força e por acreditar em mim e nas minhas capacidades mãe, pelo entusiasmo que demonstrou pelo meu trabalho e pelos abraços quando as coisas não corriam tão bem.
Obrigado por me aliviares os minutos de trabalho dolorosos, com as tuas brincadeiras Dina, pela confiança que me depositaste e que me fez acreditar ainda mais.
E obrigado a ti Hugo, por todo o teu tempo, por estares disponível a qualquer hora, pela ajuda informática excecional e pelas chamadas de atenção nas correções, mas principalmente por teres encurtado a distância várias vezes da maneira como o fizeste e me teres trazido as lufadas de ar que precisava para conseguir tudo isto.
Sem vocês nada disto teria sido possível. Obrigado!

palavras-chave

Ácido Hialurónico, Cicatriz Glial, Compressão medular, Matriz Extracelular, Regeneração.

resumo

A lesão medular é uma desordem neurológica devastadora que afeta milhares de pessoas a cada ano. E apesar de nas últimas décadas ter sido feito um enorme progresso relativamente à compreensão dos eventos moleculares e celulares que este dano desencadeia, a lesão medular ainda é uma condição altamente incapacitante e mortal para a qual ainda não há cura. Os indivíduos que apresentam lesões medulares, manifestam disfunção ou perda, temporária ou permanente, das funções motoras, sensoriais e/ou autonómicas.
Atualmente a taxa de incidência desta tipologia de lesões é de aproximadamente, 15-40 casos por milhão de pessoas em todo o mundo. Na origem destas lesões estão: acidentes rodoviários, quedas, violência interpessoal e a prática de desportos.
Neste trabalho foi colocada a hipótese de que o ácido hialurónico (HA) seja um dos componentes do tecido cicatricial formado após a compressão medular e que provavelmente seja sintetizado pelas células gliais situadas à volta da lesão, podendo ajudar na penetração da cicatriz glial, por parte das células nervosas, durante uma fase mais tardia da lesão da espinal medula.
Atualmente tem sido dada muita atenção ao restabelecimento da função do SNC, impossibilitado pelo elevado teor de proteoglicanos sulfatados na matriz extracelular. O contrabalanço do rácio entre o teor de proteoglicanos e de HA pode ser uma terapia experimental para a re-permeabilização do tecido da cicatriz glial formada após a lesão medular, possibilitando o crescimento axonal e a recuperação funcional.
Por isso, estabeleceu-se um modelo de compressão da espinal medula em ratinhos e estudou-se o tecido da cicatriz glial, em particular, a caracterização da expressão de enzimas relacionadas com o metabolismo do HA e a sua posterior concentração a diferentes distâncias do epicentro da lesão.
Os nossos resultados mostram que a lesão induzida em ratinhos produziu resultados semelhantes às lesões encontradas em humanos, tanto do ponto de vista histológico como funcional. No entanto, após traumatismo, estes animais demonstraram um mecanismo de recuperação espontânea impressionante na espinal medula resultando numa recuperação parcial da função do SNC.
Quanto ao estudo da cicatriz glial, as alterações foram detetadas na expressão do mRNA das enzimas metabolizadoras de HA, isto é, após a lesão houve uma diminuição na expressão das HAS1-2 e um aumento na expressão de mRNA da sintase HAS3 assim como das enzimas ligadas à degradação do HA, HYAL 1-2. Porém, duas semanas após LM a concentração de HA medida através do teste ELISA encontrou-se inalterada. É impossível explicar este facto apenas com a mudança na expressão das enzimas ligadas ao HA. A duas semanas pós-trauma, em resposta à LM, encontrámos HA sintetizado por astrócitos reativos e, provavelmente, por outras células, como a microglia tal como foi avançado pela co-localização de HA/IBA1^{+} e HA/GFAP^{+}.

keywords

Hyaluronan, Glial Scar, Spinal cord compression, Extracellular Matrix, Regeneration.

abstract

Spinal cord injury (SCI) is a devastating neurological disorder that affects thousands of people each year. Although in recent decades significant progress has been made in relation to understanding the molecular and cellular events underlying the nervous damage, spinal cord injury is still a highly disabling condition for which there is no curative therapy. People affected by spinal cord injuries manifested dysfunction or loss, temporary or permanent, of motor, sensory and / or autonomic functions depending on the spinal lesion damaged. Currently, the incidence rate of this type of injury is approximately 15-40 cases per million people worldwide. At the origin of these lesions are: road accidents, falls, interpersonal violence and the practice of sports.

In this work we placed the hypothesis that HA is one of the component of the scar tissue formed after a compressive SCI, that it is likely synthetised by the perilesional glial cells and that it might support the permeation of the glial scar during the late phase of SCI. Nowadays, much focus is drawn on the recovery of CNS function, made impossible after SCI due to the high content of sulfated proteoglycans in the extracellular matrix. Counterbalancing the ratio between these proteoglycans and hyaluronic acid could be one of the experimental therapy to re-permeate the glial scar tissue formed after SCI, making possible axonal regrowth and functional recovery.

Therefore, we established a model of spinal cord compression in mice and studied the glial scar tissue, particularly through the characterization of the expression of enzymes related to the metabolism of HA and the subsequent concentration thereof at different distances of the lesion epicenter.

Our results show that the lesion induced in mice shows results similar to those produced in human lesions, in terms of histologic similarities and behavioral results. but these animals demonstrate an impressive spontaneous reorganization mechanism of the spinal cord tissue that occurs after injury and allows for partial recovery of the functions of the CNS.

As regards the study of the glial scar, changes were recorded at the level of mRNA expression of enzymes metabolizing HA i.e., after injury there was a decreased expression of HA synthases 1-2 (HAS 1-2) and an increase of the expression HAS3 synthase mRNA, as well as the enzymes responsible for the HA catabolism, HYAL 1-2.

But the amount of HA measured through the ELISA test was found unchanged after injury, it is not possible to explain this fact only with the change of expression of enzymes. At two weeks and in response to SCI, we found synthesized HA by reactive astrocytes and probably by others like microglial cells as it was advanced by the HA/GFAP^{+} and HA/IBA1^{+} cells co-location.

mots-clés L'acide Hyaluronique, Cicatrice Gliale, Compression de la moelle épinière, Matrice Extracellulaire, Régénération.

résumé

Le traumatisme médullaire est une affection neurologique dévastatrice qui affecte des milliers de personnes chaque année. Bien que ces dernières décennies d'énormes progrès ont été fait par rapport à la compréhension des événements moléculaires et cellulaires qui déclenchent les dommages au sein du tissu nerveux, les dommages de la moelle épinière sont encore irréversibles et rendent les personnes atteintes très invalidées. Aucun traitement visant à remédier aux pertes fonctionnelles n'est disponible. Les gens atteints de traumatismes de la moelle épinière, manifestent un dysfonctionnement ou une perte, temporaire ou permanente, des fonctions motrice, sensorielle et / ou autonome. Actuellement, l'incidence de ce type de blessure est d'environ 15-40 cas par million de personnes dans le monde. L'origine de ces lésions sont: accidents de la route, chutes, violence interpersonnelle et pratique de sports.
Dans ce travail, nous avons placé l'hypothèse que l'acide hyaluronique (HA) est l'un des composants du tissu cicatriciel formé après une compression de la moelle épinière, qu'il est probablement synthétisé par les cellules gliales péri lésionnelles et qu'il pourrait soutenir la pénétration de la cicatrice gliale pendant la phase tardive de la LM. Actuellement beaucoup d'attention est attirée sur le rétablissement de la fonction du système SNC, rendue impossible après la LM en raison de la contenu élevé en protéoglycanes sulfatés dans la matrice extracellulaire. Contrebalançant le rapport entre ces protéoglycanes et l'HA peut être une thérapie expérimentale de la re-pénétration dans le tissu de cicatrice gliale formé après la LM, ce qui rend possible le repousse axonale et la récupération fonctionnelle.
Par conséquent, nous avons établi un modèle de compression de la moelle épinière chez des souris et étudié le tissu de la cicatrice gliale, en particulier par la caractérisation de l'expression des enzymes liées au métabolisme de l'HA et la concentration ultérieure de celui-ci à des distances différentes de l'épicentre de la lésion.
Les résultats montrent que la lésion induite chez la souris produit des résultats similaires à ceux trouvés dans les lésions humaines, d'un point de vue fonctionnel et histologique. Toutefois, après un traumatisme, ces animaux ont démontré un mécanisme de récupération spontanée impressionnante dans la moelle épinière entraînant une reprise partielle de la fonction du système nerveux central.
De manière surprenante, la quantité d'HA vérifiée par le test ELISA s'est trouvé inchangée deux semaines après traumatisme médullaire. Il est impossible d'expliquer ce fait uniquement avec le changement de l'expression d'enzymes liées à l'HA. Nous avons constaté que deux semaines après traumatisme, il ya l' HA synthétisé par les astrocytes réactifs et probablement par d'autres comme les cellules microgliales comme il a été avancé par les résultats de co-localisation de l' HA et cellules $GFAP^{+}$ ainsi que l'HA et cellules $IBA1^{+}$.

Table of Contents

Index of Figures

Index of Tables

Abbreviations

b-TGS6 - beta TNF-stimulated gene 6 protein

BDNF - Brain Derived Neurotrophic Factor

BMS- Basso Mouse Scale

BSA - Bovine serum albumin

BSB - Blood Spinal Barrier

CD44 - cluster of differentiation - 44

c-IAP$_2$ - cellular inhibitor of apoptosis 2

cDNA - Complementary deoxyribonucleic acid

ChABC - Choindroitinase ABC

Ct - Cycle threshold

CNS - Central Nervous System

Da - Daltons

DAB - 3,3'-Diaminobenzidine

DPX - 1,3-Diethyl-8-phenylxanthine

dNTP - Deoxynucleotide

CSPG - Chondroitin sulfate proteoglycan

ECM - Extracellular matrix

ELISA - Enzyme-linked immunosorbent assay

FITC - Fluorescein isothiocyanate

GAG - Glycosaminoglycan

GFAP - Glial fibrillary acidic protein

GPI - Glycosylphosphatidylinositol

GM - Grey matter

HA - Hyaluronic acid

HABP-Hyaluronan Binding Protein

HRP - Horseradish Peroxidase

HPRT - Hypoxanthine-guanine phosphoribosyltransferase

HAS 1, 2, 3 - Hyaluronan synthases 1, 2, 3

HMW-HA - High molecular weight hyaluronan

HYAL 1, 2 - Hyaluronoglucosaminidase 1, 2

IBA1 - Ionized calcium-binding adapter molecule 1

IL-12 - Interleukin 12

LM - Lesão medular/Lesion Médullaire

LMW-HA - Low molecular weight hyaluronan

mm - Millimeters

MMPs - Metalloproteinase's

MP - Methylprednisolone

mRNA - Messenger Ribonucleic acid

NF-kB - Nuclear Factor kappa B

ng - Nanogrames

NPCs - Neural precursor cells

NSCISC - National Spinal Cord Injury Statistical Center

NTSCI - Non-traumatic spinal cord injury

OCT - Optimum cutting temperature

OPC - Oligodendrocytes precursor cells

PB - Phosphate buffer

PBS - Phosphate buffered saline

PFA - Paraformaldehyde

PNN - Perineuronal nets

PNS - Peripheral Nervous system

q-PCR - quantitative Polymerase Chain Reaction

RHAMM - Receptor for HA - mediated motility

ROS - Reactive oxygen species

SCI - Spinal cord injury

SD - Standard deviation

TSCI - Traumatic spinal cord injury

TLR-2 - Toll-like receptor 2

TLR-4 - Toll-like receptor 4

TNF - Tumor necrosis factor

VEGF - Vascular Endothelial Growth Factor

WM - White matter

µm - Micrometers

INTRODUCTION

Briefly anatomy of Spinal Cord

In human being, spinal cord length is about 42-45 cm and subdivided in 5 regions: cervical, thoracic, lumbar, sacral and coccygeal which are associated with different functions (Figure 1).

There are differences in length between the bony spinal column and the spinal cord, so neurological levels of the spinal cord do not necessarily correspond to the vertebral segments, neurological segmental levels correspond to the nerve roots that exit the spinal column between vertebrae's (WHO, 2011). There are 31 pairs of spinal nerve roots: 8 cervical, 12 thoracic, 5 lumbar, 5 sacral and 1 coccygeal.

When spinal cord is damaged, the physical effect vary according to the impact site and the severity of the injury. Higher is the injury, more important is the functional loss due to the interruption of downstream spinal pathways. According to the National Spinal Cord Injury Statistical Center, the region of the spinal cord most affected in SCI is the cervical spine, occurring in 56% of all SCI cases (NSCISC, 2015).

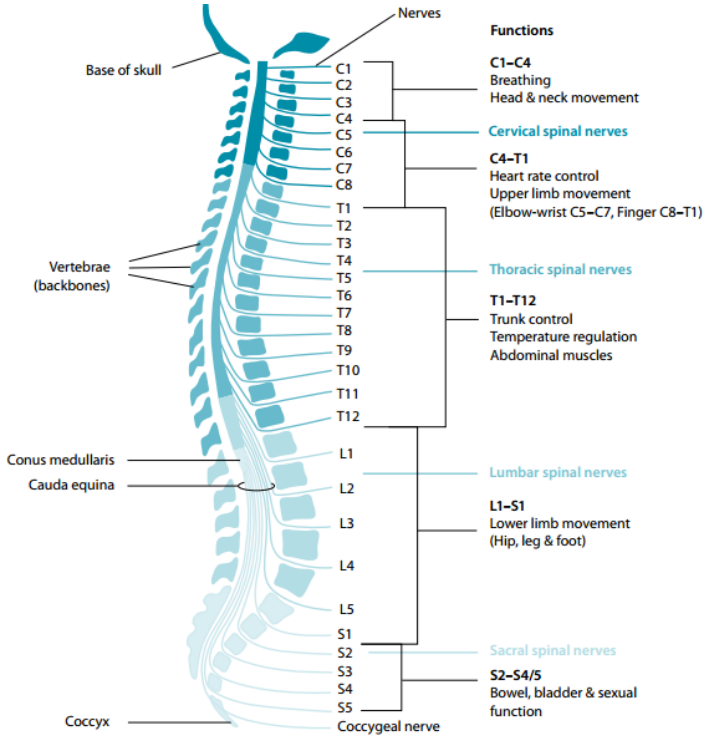

Figure 1: Organization of the spinal cord with segmental division (cervical, thoracic, lumbar and sacral) and the main functions associated (WHO, 2011).

Numbers in spinal cord injury

Spinal cord injury (SCI) remains a major public health problem worldwide (Taghva *et al*., 2012).

SCI is defined by the National Spinal Cord Injury Statistical Center (NSCISC) as any injury to the structures contained in the spinal canal, resulting in temporary or permanent loss of motor, sensory and/or autonomic function.

The Annual incidence rate of SCI, in developing countries, is 25.5/million/year cases, males with mean age of 32 years are the most affected group, accounting for approximately 82% of new SCI cases (Movaghar *et al.,* 2013).

Portugal appears higher in the list of annual crude incidence rate about traumatic SCI registering 57.8 cases per million of people (Berg *et al*., 2010).

Injuries to the central nervous system can be of two types: traumatic or non-traumatic injuries.

Traumatic spinal cord injuries (TSCI) generally result from a rapid displacement or fracture of the vertebrae that impacts the soft CNS tissue, (Jakeman *et al*., 2014).

The main causes identified for TSCI are vehicle crashes (38%), falls (30%), interpersonal violence (15%) and sports (9%) (NSCISC, 2015).

Non traumatic injuries usually involves an underlying pathology, such as infectious disease, tumour, congenital problems such as spina bifida that is abnormality linked to defective neural tube closure during embryonic development, and stroke, a non-haemorrhaging stroke, caused by a sudden arterial occlusion that disrupts blood flow to tissue, leading to tissue necrosis in the territory of occluded artery (Moshayedi *and* Carmichael, 2013)

The incidence of NTSCI varies by both age and sex. As with TSCI, incidence rates of NTSCI are higher among males than females. NTSCI incidence increases consistently with age with risk influenced by the increase of ill health with increasing age (WHO, 2011).

The number of NTSCI is difficult to know because there are many different causes, and there is no unique big registry where all the information is gathered. But according to an australian study the incidence rate of NTSCI is almost double, estimated in 26/million compared to 15.3/million adults/year reported to TSCI (New, 2006).

Current treatments

Currently the treatment given to patients with acute SCI vary according to the local/regional protocol available due to the lack of medical consensus.
Previous clinical trials have shown benefits of steroids administration and administration of high doses of Methylprednisolone (MP) within the first 8 hours after traumatic injury, reducing the pain and the inflammatory response. This last treatment is recommended by National Acute Spinal Cord Injury Study (NASCIS) to use MP as standard procedure in the clinical practise. On the contrary, there are also evidences showing that high-dose steroids are associated with harmful adverse effects (Bracken, 2012). For instance, high dose of MP have been associated with side effects such as anxiety, dizziness, mental depression and an increased risk of infectious and metabolic complications (Suberviola *et al*., 2008). Surgical decompression prior to 24 hours after SCI, also can help in vascular circulation being mentioned as safety procedure and is also being associated with some improved neurologic outcome (Fehlings *et al.,* 2012).

Regeneration of peripheral nervous system and central nervous system

CNS regeneration after damage is not simple because it does not own the same repair capacity as the peripheral nervous system (PNS). When damage to CNS or PNS occurs, the axon is cut, separate from neuron's cell body undergoing wallerian degeneration distal to the injury. In the CNS, many factors synthetized after trauma inhibit axonal regrowth and do not promote the re-shaping of the normal spinal tissue architecture. Among these inhibitory factors, the components of the glial scar, i.e. oligodendrocyte precursors, reactive astrocytes, microglial cells, inflammatory cytokines, extracellular matrix proteins such as CSPGs have been clearly pointed out as the main inhibitors of axonal regrowth. Wallerian degeneration in the PNS initiates removal of myelin debris and axons through the recruitment of macrophages into the injured area.
Axonal skeleton thus disintegrates as the axonal membrane of the axon, although the outer layer of Schwann cells that surround the axons does not disintegrate giving rise to a hollow tube that allows these cells to attract the axon sprouts from the proximal end to the distal end of the damaged axons, through growth factors synthesis. The efficient innate-immune response helps turning the PNS tissue into an environment that supports axon regeneration (Alovskaya *et al.,* 2007).

Primary and secondary damage to spinal cord

The lack of capability to CNS regeneration is mainly hampered by the second event that occur after the primary injury to the spinal cord, because SCI follows a biphasic process where the secondary biological events sets in minutes after injury and lasts for weeks or months (Table 1) (Oyinbo, 2011).

The primary injury is the mechanical insult itself that occurs during the accident due to compression, stretching and involves immediate rupture or crushing of neural tissue and vascular elements (Rowland *et al,* 2008).

This fact initiates a cascade of secondary events leading to hemorrhage, hypoxia, strong inflammatory response, astrogliosis, apoptosis, electrolyte deregulation and reactive oxygen species generation gathered in the term “secondary injury” characterized by progressive rostro-caudal extension of the primary lesion, causing further damage to spinal tissue (Marques *et al*., 2009).

Table 1: Phases of SCI and molecular/cellular events developed in each phase (Rowland *et al.*, 2008).

	Time After SCI				
Phases and Key Events	≤2 Hours	≤ 48 Hours	≤14 Days	≤ 6 Months	≥ 6 Months
injury phase	primary immediate	early acute	secondary subacute	intermediate	chronic/late
key processes and events	primary mechanical injury traumatic severing of axons grey matter hemorrhage hemorrhagic necrosis microglial activation released factors: IL-1β, TNFα, IL-6, & others	vasogenic & cytoxic edema ROS production: lipid peroxidation glutamate–mediated excitotoxicity continued hemorrhage & necrosis neutrophil invasion peak BBB permeability early demyelination (oligodendrocyte death) neuronal death axonal swelling systemic events (systemic shock, spinal shock, hypotension, hypoxia)	macrophage infiltration initiation of astroglial scar (reactive astrocytosis) BBB repair & resolution of edema	continued formation of glial scar cyst formation lesion stabilization	prolonged Wallerian degeneration persistence of spared, demyelinated axons potential structural & functional plasticity of spared spinal cord tissue
therapeutic aims	neuroprotection	neuroprotection immune modulation cell-based remyelination approaches glial scar degradation		glial scar degradation	rehablitation neuroprostheses

Despite cellular and molecular mechanisms underlying secondary spinal cord injury are still not completely understood (Zhou *et al.,* 2014), it is known the importance to reduce the neuronal loss induced by the secondary damage, mainly because the degree of

neurologic disability after spinal cord trauma depends of the extent of neural element loss and the remaining function of the residual neural tissue (Oyinbo, 2011).

ECM in the CNS

A tissue, whatever it is, is constituted by a certain kind of cells which have specialized in certain functions, constituting organisms. On unicellular creatures, their cellular wall is the barrier between them and the exterior environment whereas in our organism, cells are integrated and surrounded by an environment called extracellular matrix (ECM). The ECM is formed by components synthetized by cells, being each ECM specific for certain group of cells in a certain condition.

ECM occupies 20% of the volume of the adult CNS and is produced and assembled by neurons and glial cells (Sherman *and* Back, 2007).

Extracellular matrix in CNS is a meshwork of hyaluronan, sulfated proteoglycans and tenascin R. (Wakao *et al.*, 2011). HA works as a backbone to sulfated proteoglycans linkage, which are linked to one or more sulfated GAG chains. Tenascin-R binds to sulfated proteoglycans domains, forming homodimers or trimers. The complexes are secured to the linear HA sugar by link proteins, allowing a stable substrate for cells (Gaudet *and* Popovich, 2014).

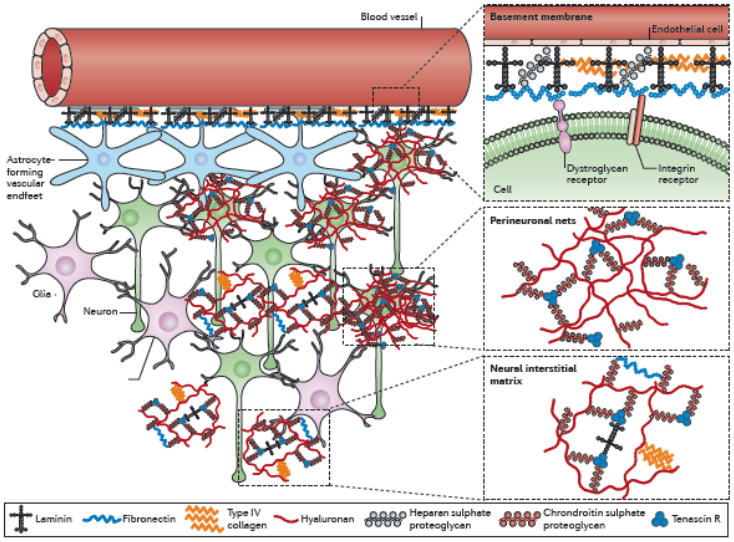

Figure 2: Different ECM composition in the CNS. In basement membranes, ECM surrounds endothelial cell-vessels, in a condensed way as perineuronal nets (PNN) around the cell bodies and proximal dendrites of neurons. In neural interstitial matrix ECM are diffusely distributed between the neuronal or glial cells of the CNS parenchyma (Lau *et al*., 2013).

Initially thought that ECM had simply functions as contributing to structural stabilization of

neural processes and synaptic contacts in central nervous system and in tissue elasticity. Actually ECM is known to regulate processes in cell development, neuronal activity and axonal growth (Soleman *et al.*, 2013).

Functions and organization of ECM differs depending of the CNS sub-region: perineuronal nets (PNN), neural interstitial matrix and ECM from basal lamina (Figure 2).

Perineuronal net (Figure 3) is a layer of condensed pericellular matrix composed of ECM molecules strongly expressed around cellular bodies and proximal dendrites of some neurons in CNS (Kwok *et al.*, 2011). In PNNs, ECM is attached to hyaluronan synthases molecules presents in the cell membrane.

This PNN is necessary to protection of highly active neurons in response to high neuronal electrical activity. It helps also in inhibiting the structural rearrangements at synapses, contributing to the maintenance of neuronal networks, controlling neuronal plasticity (Schreiber *et al*., 2013).The disruption of the PNN components through the enzymatic digestion of HA or chondroitin sulfate GAG chains resulted in destabilization of this structure and enhanced plasticity (Soleman *et al*., 2013).

Quite similar dense ECM structures are formed at perinodal regions along axons in the white matter tracts, where they also enhances axonal conduction efficiency (Burnside *and* Bradbury, 2014).

In basal lamina a distinct ECM is found with more components like collagen type 4, fibronectin, perlecan, dystroglycan, and laminin-nidogen complexes, whose functions are related to blood-brain barrier maintenance (Lau *et al*., 2013).

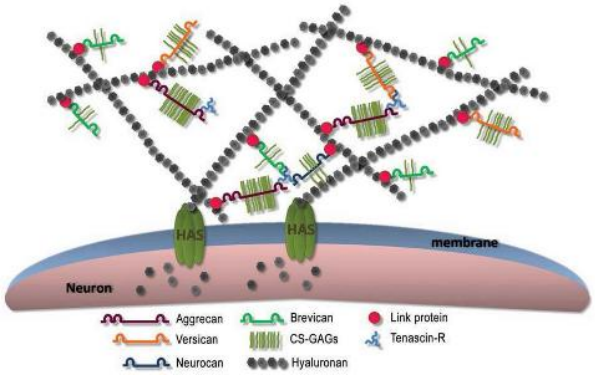

Figure 3: synthesis and secretion to the perineuronal space by HAS enzymes present in the inner membrane of neurons. In the extracellular space, HA function as the backbone where are the link proteins that stabilize the binding of proteoglicans to HA (Kwok *et al*., 2011).

Hyaluronan and his receptors (CD44, RHAMM, TLR-2,4)

Hyaluronan or hyaluronic acid (HA) is a linear non-sulfated glycosaminoglycan of long chain composed by repeated disaccharide unites of N-acetyl glucosamine and glucuronic acid (Figure 4), representing one of the major constituents of the extracellular matrix in the CNS (Khaing *et al*., 2011).

HA is found ubiquitously in the body, skin is the organ with the greatest amount, accounting for 50% of the total body HA (Papakonstantinou *et al*., 2012). It is also widely distributed throughout the developing and adult CNS being produced predominantly by astrocytes and to a lesser extent by oligodendrocytes, neurons and microglia (Jakeman *et al*., 2014).

It acts as a structural component of the extracellular matrix as well as a mediator of various cellular functions due to its capacity to induce cell signalling through multiple transmembrane receptors involved in nervous system responses to injury, influencing cell proliferation, differentiation, migration and survival (Yang C. *et al*., 2012).

However physiological functions of HA change depending on its size (“high molecular weight” - HMW HA versus “low molecular weight” - LMW HA), sometimes demonstrating opposing actions. It can have pro- or anti-inflammatory properties, promote or inhibit cell migration, activate or stop cell division and differentiation (Cyphert *et al*., 2015).

HMW beyond the structural role, silences inflammation, angiogenesis and neural differentiation (Moshayedi *and* Carmichael, 2013).

It has been shown that injury to the spinal cord can result in degradation of native HMW-HA into LMW forms (Struve *et al*., 2005). Struve and co-workers demonstrated that the consequence of native HA degradation was the proliferation and activation of astrocytes through CD44 receptor activation.

The opposite response were seen in the presence of HMW-HA in a culture of astrocytes demonstrating reduction in cell proliferation and in the amount of astrocyte-derived CSPG production (Khaing *et al*., 2011).

In rat model of spinal cord hemisection injury, Khaing *et al.,* 2011 showed significant reduction in the number of immune cells detected at the lesion site, significant lower CSPG expression and a decrease in astrocytic response after implantation of HMW-HA hydrogels.

This experiment suggests that HMW-HA limits astrocytic activation by keeping them in a quiescent state through HMW hyaluronan-CD44 interaction. When damage occurs, HA is degraded and the astrocytes becomes reactive, proliferates and origins scar formation.

Slevin and co-workers (2007) also reported the conflicting functions of HA. The native high molecular weight HA is anti-angiogenic whereas low molecular weight demonstrated to be angiogenic, stimulating endothelial cell proliferation and migration following activation of CD44 and RHAMM.

Sloane and co-workers (2010) have reported that HA products generated by hyaluronidase activity, are able to bind TLR2 on the surface of OPCs, inhibit their maturation, prevent their differentiation and block axons remyelination.

One hypothesis to explain this contradictory functions of HA come from the study of Yang C et al., 2012, where they explain that native hyaluronan induce CD44 clustering that is attenuated when HA is replaced by low molecular forms.

Properties of HA have been used in several ways, also as a medium of inclusion ("scaffold") for cell therapy, in a study where neural stem progenitor cells (NSPC) were injected within a combination of HA and modified methyl cellulose hydrogel, in a subacute model of rat SCI. Results demonstrated improvement of graft survival, increased oligodendrocyte differentiation, reduction in lesion cavity and improved behavioural recovery (Mothe *et al.,* 2013).

Together, all studies support the idea that HA and multiple HA receptors are involved in responses of CNS to injury and in different cellular behaviours.

The major surface hyaluronan receptor implicated in intercellular and cell-matrix adhesion, cell migration and signalling is CD44. CD44 is a transmembrane glycoprotein mediating cell responses to the extracellular microenvironment. These functions are linked to the cytoplasmatic tail, influencing cell migration through his cleavage by metalloproteinases, which results in release of cells bound to HA (Dzwonek and Wilczynski, 2015). CD44 is expressed by astrocytes, neurons, oligodendrocytes, neural stem cells and endothelial cells. In endothelial cells, the role of CD44 is to promote the crossing of lymphocytes across CNS vascular endothelium (Winkler *et al*., 2013).

RHAMM, receptor for hyaluronan-mediated motility, is another HA binding receptor, expressed by subsets of neurons and glial cells, especially oligodendrocytes. RHAMM is located on the cell surface as a GPI-anchored protein and in the cytoplasm (Sherman *et al.,* 2015).

HA binds to RHAMM and influence cell growth and glial cell migration due to the complex network of signal transduction events with the cytoskeleton structures (Papakonstantinou *et al*., 2012).

Both TLR-2 and TLR-4 bind HA. TLR are expressed by microglia and astrocytes and it is being demonstrated the binding of LMW-HA to TRL-2 leads to inhibition of OPC

maturation and consequent failure in axon remyelinization (Sloane *et al*., 2010).

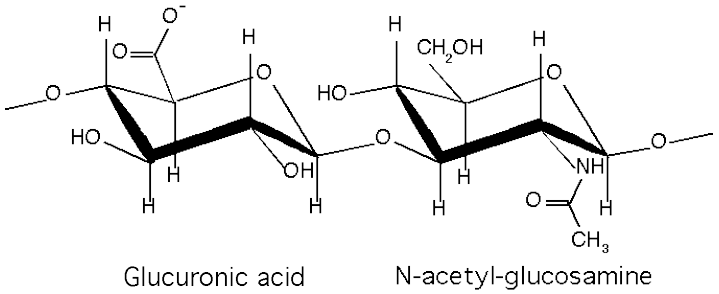

Figure 4: Chemical simple structure of HA composed by repeating disaccharides of N-acetyl glucosamine and glucuronic acid (Onken, 2011).

HA Synthesis and degradation

Mammalian hyaluronan synthesis is accomplished by three membrane-bound glycosyltransferases isozymes, hyaluronan synthases (HAS) 1, 2 and 3 located at the inner face of the plasma membrane. HA is secreted to the extracellular space as a linear molecule. Despite their similarities, the three hyaluronan synthases produce HA of varying molecular mass. HAS 1 and HAS 2 produce the larger polymers > $2x10^6$ Da with a reduced synthesis rate while HAS 3 produce shortest HA polymer size with a molecular mass lighter than $2x10^5$ Da and greater synthesis rate (Sherman *and* Back, 2007).

The HAS genes have a different temporal pattern of expression during the morphogenesis. Expression of HAS2 at all stages of embryogenesis is explained by lethality of HAS2 knockout mice linked to vascular defects whereas in double knockouts HAS1 and HAS3, mice are viable (Dicker *et al*., 2014).

In mammals, hyaluronidases consist of six HYAL family members: HYAL 1-4, PH20, and HYALP1 that differ in their cellular localization. The general mechanism, in somatic tissues, accepted for HA degradation is that HMW-HA bind to his transmembrane receptor CD44 and GPI anchored-Hyal 2 reduces the HA molecule in size to products with 50 disaccharide units that will be internalized and transported to lysosomes for further degradation carried out by intracellular Hyal-1(Sherman *and* Back, 2007).

Nowadays, we still do not know how HA degradation is regulated in the normal CNS and after CNS injury. We only know that HA degradation happens soon after SCI, leading to the degradation of HMW-HA to LMW-HA. This last one seems to amplify the inflammatory response by initiating inflammatory signalling in macrophages or microglia and increasing expression of inflammatory cytokines (like TNF alpha and IL-12). It also recruits activated lymphocytes T into sites of inflammation from the blood vessels by up-regulating their CD44 (Popovich *and* Gaudet, 2014). In figure 5 we can see the feed-forward cycle that is

induced by SCI.

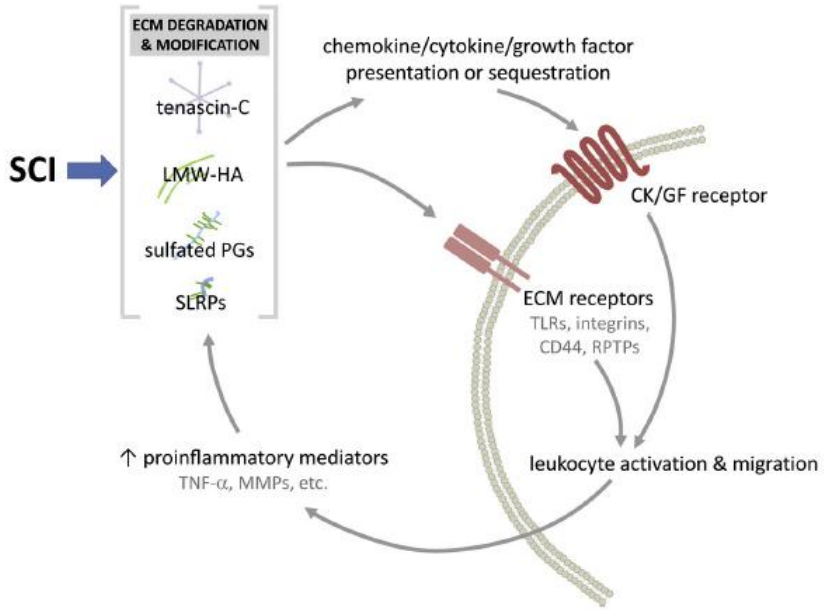

Figure 5: Spinal cord injury induces changes in ECM composition, like the fragmentation of HMW-HA and modification of tenascin-R, molecules that bind to ECM receptors or cytokines, chemokines causing the activation of this receptors and migration of the cells. The accumulation of inflammatory cells leads to the secretion of pro inflammatory mediators as TNF-alpha and metalloproteinase (MMP) that further degrade ECM molecules (Popovich *and* Gaudet, 2014).

Besides the ECM modification, cells intrinsic to the spinal cord contribute to inflammation, through the activation of astrocytes and microglia near the lesion that starts to proliferate and release inflammatory cytokines.

Astrocytes undergo morphological and biochemical changes, they become reactive and increase their expression of GFAP and CD44 at their surface (Silver *and* Miller, 2004). They become hypertrophic and accumulate within the lesions where they are part of the glial scar tissue. Although being detrimental during the scarring, reactive astrocytes are required in the early phases post-SCI by protecting unaffected surrounding tissues from damaged tissues, limiting extension of the lesion; they notably accumulate at the margins of the lesion epicenter to help in the reestablishment of the blood spinal barrier (Yuan *and* He, 2013).

Recently the involvement of HA in CNS injuries has aroused interest and there are many studies that investigate the therapeutic effect of HA oligosaccharides action.

Wakao and co-workers (2011) demonstrated for the first time that HA4 improved motor function recovery after SCI, after investigation of several HA oligosaccharides (HA2-HA12). After HA4 treatment, they observed a decreased accumulation of IBA1 positive cells in a lesion 2 weeks after SCI, and the enhanced axonal regeneration/sprouting accessed by corticospinal tract tracer fiber counts.

Wang and co-workers found that HA tetrasaccharides (HA4), when added to astrocytic cultures were able to induce astrocytes to express more neurotrophic factors as BDNF and VEGF, promoting repair of damaged neurons and oligodendrocytes. They also found that HA4 induce NF-kB and c-IAP_2 to suppress H_20_2 induced apoptosis in neuronal cultures. When the HA4 polymer sheets implantation was done, after compression of the spinal cord, results demonstrated that HA4 level was increased in the cerebrospinal fluid and associated with behavioural recovery of rats.

Also Wang and co-workers *(*2015) in the continuation of their study, they found that high expression of VEGF and BDNF in astrocytes induced by HA4 were inhibited by blocking the receptors CD44 and TRL-4, suggesting that is through interaction with these receptors, HA4 exerts its therapeutic effect.

Glial Scar formation

Classified as one of the main physical and molecular barriers to regenerating axons, the glial scar forms, following injury, as neural wound healing response (Figure 6).

It is formed by a dense meshwork of reactive glial cells, mostly by reactive astrocytes that up regulate high levels of the main axonal inhibitory molecules, CSPGs that persist for several weeks after CNS injury, preventing axon remyelination and restricting axon plasticity, essentials for regeneration (Sharma *et al*., 2012).

However, reactive astrocytes also provide essential activities in protecting tissue and preserving function after SCI, demonstrated by Faulkner and co-workers (2004). These authors used a transgenic mouse model where proliferating astrocytes can be ablated, absence of reactive astrocytes early post-SCI considerably worsens morphological and functional outcomes than in wild type mice: failure of BSB repair, increased leukocyte infiltration, extended spinal tissue disruption, severe demyelination, more neuronal and oligodendrocyte death, and more pronounced motor deficits, even in small injuries.

Infiltration of immune cells, such as microglia and macrophages, meningeal cells, and fibroblasts not usually found within CNS, are activated during different times in the inflammatory process and involved in the process of glial scar formation (Soleman et al., 2013) that along with inhibitory molecules, like CSPSs, prevent the access to the site of injury through the establishment of the inhibitory microenvironment that prevents the regeneration of damaged axons and inhibits synaptic plasticity, essential for neurological repair.

Efforts to rend the microenvironment more permissive had discovered that removal of the

GAG side chains of CSPGs using the bacterial enzyme chondroitinase ABC increase plasticity and enables a certain degree of axonal regeneration (Cafferty *et al*., 2007). Subsequently increased axonal sprouting lead to a promotion of functional recovery in animal models of SCI treated with local infusion of ChABC (Wang *et al*, 2011).

The classical method of administration of ChABC is through intrathecal injection but is difficult to execute due to the limitations such as the enzyme ChABC thermal sensitivity, reducing the activity after 5 days maximum at 37ºC, and the constant needed of delivery due to the fact that CSPG are chronically upregulated during weeks. So, with the need to have a more stable enzyme or an efficient method for the ChABC delivery, the translation of chondroitinase therapy to clinic is not possible.

Last works in this area investigated the use of a thermostabilized enzyme ChABC administered through a lipid microtube-hydrogel scaffold system of delivery (Lee *et al*., 2010). The study results showed low levels of CSPG for 6 weeks, after SCI in vivo, and the improved locomotor behaviour, correlated with axonal sprouting at the lesion site.

Recently, another type of work was reported study to promote axonal sprouting beyond the glial scar through the administration of a DNA enzyme to XT-1 mRNA, enzyme that initiates GAG-chain formation, reducing XT-1 mRNA level after a dorsal hemisection of the spinal cord, promoting corticospinal tract regeneration and improving behavioural outcome after spinal cord injury (Koenig *et al*., 2015).

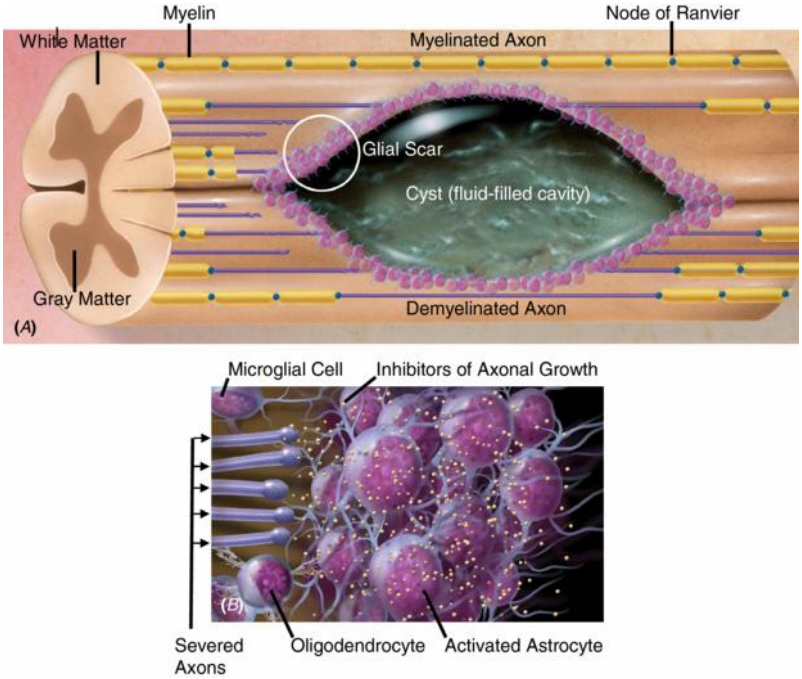

Figure 6: Scheme representing a fluid-filled cavity surrounded by glial scar composed by reactive astrocytes that produce CSPG (inhibitors of axonal growth), accumulating at the injury site being the main cause for failure of axon regeneration (http://www.shannonassociates.com/artist/edmondalexander/category/21#url=3184).

Mice compression model at T9 vertebrae

In our study we used animal model because it allows us to mimic the anatomical and biological consequences of SCI, where it is practically or ethically difficult to use humans.
Despite being not the most widely animal model used in SCI research, mouse models have been implemented in SCI research allowing the use of knock-out animals for genes-of-interest.
Thoracic region was chosen as the region of injury. It is more commonly used in experimental models because it does not threaten vital functions such as in cervical lesions, however humans usually present SCI at the cervical region and therefore the site of injury can greatly affect the pathology and the severity of the injury in a clinical setting.

Objective of the study

With this study we intended a better understanding of the glial scar tissue composition, with focus on hyaluronan, one of the main component in extracellular matrix, after compression-induced to the spinal cord of mice.
Firstly the mouse compression model at T9 region of the spinal cord was set up, followed by morphological characterization of the created lesion, comparing to animals submitted to laminectomy, working as the control group. Next our attentions were focused on hyaluronan, observing the mRNA expression of the HA related enzymes post-injury relating these results with hyaluronan quantification in lesion epicenter and adjacent regions of the spinal cord.

MATERIALS AND METHODS

Ethics statement

All experiments were performed in accordance with the approved animal protocols and guidelines established by University of Namur Animal ethics committee (Belgium).

Animals

Young adult male C57Bl6J mice with 10-16 weeks old, with body weight range 20-30 g, used in this study, were obtained from Janvier Company and from the university breeding.

Surgical procedures

All surgery was done under sterile conditions and the surgical procedures were performed under general anaesthesia with ketamine 100 mg/ml (Ketamine 1000 Ceva®) xylazin 20mg/ml (XYL-M® 2% VMD) in 0.9% physiological serum.

The dose was injected by intraperitoneal injection about 150 µL/20g. Once mice were anesthetized, the dorsal region (over the first two thirds to the spinal cord) was shaved and the area cleaned with an antiseptic solution, betadine ®, and a sterile compress to ensure antisepsis of the skin for the chirurgic act. Instruments used in the surgery were placed in a bead sterilizer (Steri 250 Simon Keller AG) at 250°C.

The animal was placed under a stereoscopic microscope (Olympus SZX9) for the surgery and core body temperature was maintained at 37ºC by the use of a plastic heating plate.

Once anaesthetic depth was reached, a longitudinal section was made from the elevation of the curvature of the back to the neck with a scalpel.

Next, it was crucial localize two anatomical points of reference: First the blood vessel vascularizing the hibernating gland and second, the tendons of the paravertebral muscles. Our vertebra T9 was localized between this two reference points.

After cutting the connective tissue carefully, to avoid the damaged of the blood vessel of the hibernating gland, we cut the paravertebral muscles longitudinally using a scalpel and we dissected out the muscles between them to access the spine.

Once we reached the spine the vertebra T9 was identified using a ladder of 5.6 mm length to access the right place to perform a laminectomy, in other words, to removing the dorsal aspect of the T9 vertebrae. The distance chosen for the ladder was the distance between

the blood vessel of the hibernating gland (perforate thorax between T5 and T6) and the T9 vertebra found in the literature (Harrison *et al.*, 2013).

After localizing the T9 vertebrae, we needed a rodent-clip to cut out the bone and let the spinal cord accessible to induce compression injury.

Compression was produced by inserting the forceps between the lateral sides of the cord and vertebral walls, they were held closed for different times of 5, 15, 30 or 60 seconds and then removed. In some cases, it was visible bruising of the spinal cord, but in a few animals bleeding into the space above the spinal cord obscured direct visibility of the cord. The control animals, or group laminectomy, received the same surgery and a laminectomy was executed but no compression was made to the spinal cord.

The wound was closed by suturing the vertebral muscles with absorbable line followed by closing the skin with wound clips for both groups.

Animal care

Pain associated with the surgery was managed with buprenorphine 0,05mg/kg (Vetergesic® 0.3 mg/ml Ecuphar) administered subcutaneously immediately after operation, 12h and 24 h. After surgery animals also received a subcutaneous antibiotic injection, firstly Cefazolin (SANDOZ® 1g Cefazolin sodium) that was substituted later by enrofloxacin 5%, dose 5mg/Kg (Baytril® Bayer) daily during five days and repeated if signs of infection were detected. Ringer's solution, 1 ml (lactate and physiological serum solution) was injected subcutaneously on the day of the surgery and at later days if animals showed signs of dehydration.

Mice were placed on a warming pad for assure the optimal body temperature until they were awake. Once fully conscious, they were examined to confirm bilateral paralysis of the hindlimbs. They returned to their home cages with free access to food and water.

All the animal's bladder were manually expressed twice a day until them become self-expressing.

Mice were also weighed and checked daily for any signs of distress, through the filling of the welfare data sheets with a score in the end between 0-6 (0 corresponding to better state of health and 6 to the worst state that obliges to the sacrifice of the animal) until the sacrifice day.

Behavioural analysis

Mice were evaluated using four behavioural tasks selected to asses hindlimb function: Rotarod, grip strength, hanging wire and Basso Mouse Scale open field score.

Grip strength

This test was designed to assess forelimb motor function based on the ability of the animal to exert a pulling force on a metal grid attached to an electronic grip strength meter. However, our aim was assess the hind limb motor function and we had to readjust the test to our needs.
For the assessment of the remain muscular force in hind limbs after spinal injury, we tested once a week, during 6 weeks. Each trial consisted of 3 trials for measure the force of the 4 limbs and 3 trials for measure the force of the forelimbs. Next we made the average of measurements and we subtracted the two values to obtain the force of the hind limbs.

Hanging wire

In this exercise, animals were introduced inside a cylinder with a grid placed in one of the extremity. Cylinder was placed at 30 centimetres of height. When returned, mice had to remain attached to the grid, until one minute maximum.
The time was recorded and the average of three trials was calculated for each animal.
This test was realized once a week during 6 weeks post-injury.

Rotarod test

Rotarod test was performed to assess balance and ability to coordinate stepping. In this test animals were placed in a multiple lane rotarod device in a constant acceleration from 4 to 40 rpm in a maximum time of 5 minutes. Animals were scored on seconds to fall.
This exercise required training once a day, during 5 days - two weeks before the surgery. In this first period we didn't recorded data. But after the habituation period, we submit mice twice a week, starting 1 week before surgery and we made the average of three trials per mice, to determinate the value correspondent to the best performance of mice before surgical intervention. After the surgery, mice were tested once a week until 6 weeks.

Three trials were scored individually and averaged for a final score per session.

Basso Mouse Scale open field score (BMS)

We used this scale because it is a broadly-recognized locomotor rating scale for mice and because basically our objective were to evaluate gross voluntary use of the hind limbs in the locomotion of the animals. This nine point scale provided the phases of locomotor recovery and features of locomotion with focus in gross aspects of the hind limb function. Mice were evaluated by two blinded observers and received a score for the movements of the hind limbs in our thoracic compression model in which the points mean: (0) no ankle movement, (1) Slight ankle movement, (2) larger ankle movement, (3) dorsal walking or plantar paw placing, (4) occasional plantar walking, (5) frequent plantar walking without coordination or a little bit coordinated, (6) walking frequent and a little bit coordinated with the paws parallels to the body or generally coordinated but with the paws in rotation , (7) walking frequent and coordinated with the paws parallels to the body in the initial contact with the ground but in rotation after paws off the ground or if the paws are always parallels to the body but the trunk are seriously instable, (8) walking frequent and coordinated with the paws always parallels to the body but the trunk are average instable or the trunk is normal but the tail is lowered or up and down, (9) this final score indicates the normal locomotor mobility with stability of the trunk and perfect performance.

Animals were evaluated after surgery, daily up to 6 weeks post-injury.

The score of the hindlimbs were recorded as general per animal (left and right hindlimb), obtaining a BMS score. Then, the mean of the group was calculated.

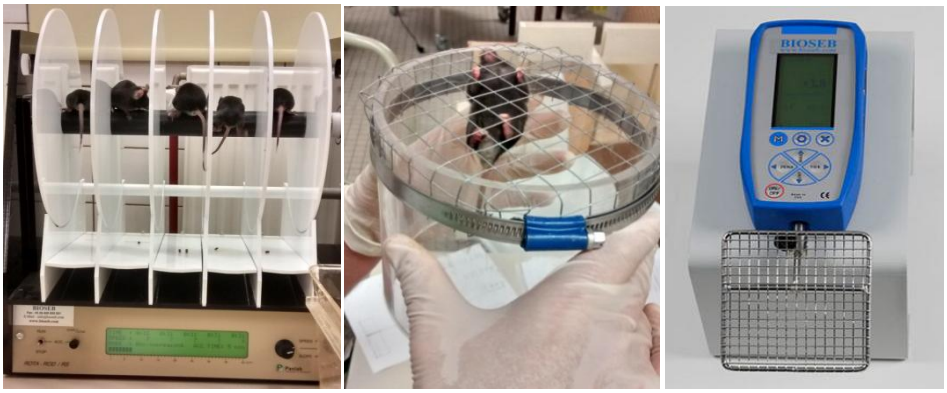

Figure 7: Behavioural tests representation, from left to right, rotarod, Hanging wire and grip strength.

Experimental design

Our working time line was performed as above:

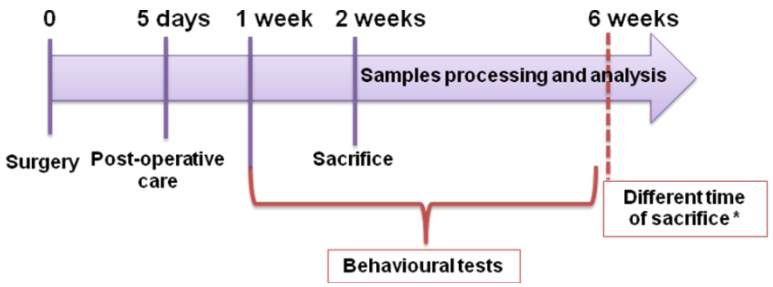

Figure 8: Time line of our work, beginning with the mice surgery followed by 5 days of post-operative cares. At 2 weeks sacrifice were executed with consequent sample processing and analysis. However we had a second group of mice that were submitted to compression of the spinal cord but it group has a different sacrifice time, performing behavioural testes from 1 week till 6 weeks after injury.

After having set up the compression injury, we splitted our pool of animals into laminectomy group (n=15) and compression group (n=15). In each group we made various samples treatments according to the intended analyses: morphologic analysis (n=5), HA concentration, ELISA (n=5) and mRNA expression of HA metabolizing enzymes, qPCR (n=5).

Tissue preparation

For the lesion characterization, two weeks after surgery, mice were anesthetized and submitted to transcardial perfusion using physiological serum until the liver changed colour to yellowish, then we perfuse with 4% paraformaldehyde in 0.1M phosphate buffer (PB) at PH 7.4, to fix the tissues.

After dissection to the spinal cord using a rodent-clip to destroy the bone and avoid the damage of the spinal cord tissue, the lesion epicenter was marked with ink.

Next the sample was post-fixed overnight at 4ºC, in 4% paraformaldehyde, followed by one hour in distilled water and then stored at 4ºC in a 30% sucrose in PB solution until the samples sank. After that, pieces of 6 mm long with 3 mm of each side of the epicentre were cut, included in OCT (Tissue-Tekr SAKURA) and refrigerated at -25°C.

Spinal cords were frozen and then cross-sectioned in a refrigerated ambiance, using a cryostat at -25ºC and 30µm thickness.

Serial sections were done and slides were stored at -25°C until staining and analysis.

For the samples embedded in paraffin, we used the same fixation with the spinal cord harvested and soaked in 4% PFA at 4ºC, overnight but next we did an immersion in absolute methanol followed by an automatic device (automatic system Sakura-Tissue Tek-Vip) that works under pressure with standard temperatures and agitation for a complete dehydration of the samples followed by coating in paraffin at 60ºC.

Samples were sectioned in a microtome (Leica) and attached to the blades with a drop of water heated on a hotplate.

For quantitative real time PCR (q-PCR) and ELISA assay, spinal cord tissues were collected also two weeks after injury with perfusion with cold physiologic serum. After the harvest of the samples we cut them in 5 pieces (rostral+1, rostral, epicenter, caudal, caudal +1) with 4 mm each one and we introduced the pieces within tubes dipped in liquid nitrogen for snap-freezing (Figure 9). Samples were stored at -80ºC until q-PCR and ELISA-like assays.

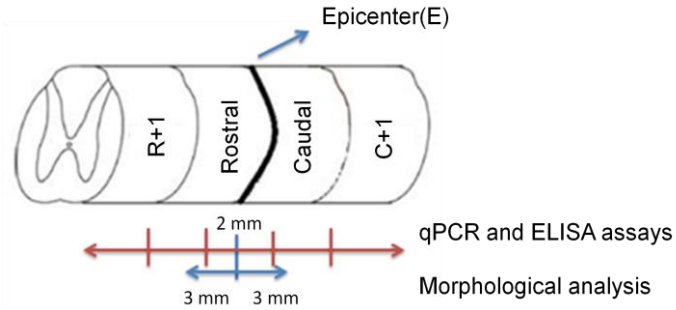

Figure 9: Scheme of the spinal cord portions used in this study. It is represented the several segments and the respective length intended for each analysis. For morphological analysis, OCT inclusion or paraffin coating, we cut a fragment of 6 mm (3 mm each side of epicenter). For gene expression analysis, qPCR, or ELISA assay we cut 5 different fragments: epicenter (E), rostral (R), caudal (C), more rostral (R+1) and more caudal (C+1) with 4 mm length each one. For epicenter segment we cut 2 mm each side.

Histological staining

Histological staining Eriochrome C with counter-staining Cresyl violet was performed to respectively visualize white matter and gray matter structures and therefore to quantify and the lesion extension.

Before staining, cryostat sections at -25ºC needed to dry at room temperature during some hours and then heated in the oven, during 30 minutes at 48°C. Sections were left to room temperature a couple of minutes and next immersed in different baths (toluol, methanol 100%, 95%, 70% and tap water) for rehydratation. Next, they were dipped for 1 minute and 45 seconds in Eriochrome C (Sigma) (10% ferric chloride – sulfuric acid 0.6% - 0.8g EC) followed by tap water and next the differentiation in ammonium hydroxyde

during 5 minutes with a rapid passage in distilled water.
For the counter-staining, we used Cresyl violet 0.4% during 1 minute and a differentiation with an increasing concentration of ethanol baths 70%, 95% and 100%.
Finally, slides were immersed in toluol and coverslipped using DPX mounting medium.
During the histological staining we lost a lot of cuts in the several baths realized, despite our careful in previously well drying and heating the blades.
The tissue thickness revealed not appropriate to the blades manipulation and we did another group of samples coated in paraffin, giving us the option to cut with smaller thickness-6 µm, increasing the adherence of the cut to the blade.
For the new group we used paraffin in sample inclusion medium; as consequence we augmented the time of Eriochrome C staining to 30 minutes and cresyl violet to 1 hour. The other steps remain the same.

Lesion histology and Motor neuron counting

With Eriochrome C/Cresyl violet staining, total and lesion area of each section were delimited and measured using Image J Software. In sections with injury, the anatomical structure of the spinal cord was not conserved and we could see damaged tissue. To the section with the highest percentage of damaged tissue we identified it as the epicentre.
We also calculated the lesion volume using *Cavalieri* estimator of volume, as shown above and as indicated in Nicaise *et al*., 2012.

$$V=[\sum(A1+A2+\ldots A_n) \times D] - [A_{max} \times Y]$$

For counting total number of thoracic motor neurons, we used the sections stained with Eriochrome C/Cresyl violet. In this exercise, the microscope objective of 10x magnification was used. First we draw an imaginary line that separated the dorsal and ventral horns of spinal cord and we counted the motor neurons with an identifiable nucleus presented in grey matter of the ventral horn below the central canal.

Staining of HA

With the aim to confirm and better understand the distribution of HA in injured and healthy spinal cord tissue we used an hyaluronan binding protein (HABP), b-TGS6 (cordially given by Halozyme Therapeutics, San Diego, California, USA) coupled with biotin and a fusion molecule streptavidin-FITC (dilution 1/500, Vector laboratories, Inc., Burlingame), for the revelation.

As positive controls human and mouse skin were chosen, and for negative controls we incubate spinal cord tissue sections with PBS – 0.2% BSA – 0.1% Triton rather than the primary antibody.

Initially we realized one washing step of the blades in PBS followed by the immersion in glycine, for 3 times during 2 minutes and a saturation step in PBS-0.2% BSA- 0.02% Triton per 1 hour at room temperature. Then, we incubated sections with the HABP b-TGS6 (dilution 1/500) in a humidified chamber, overnight at 4°C.

Samples were rinsed next day in PBS-0.2% BSA- 0.02% Triton and incubated with the streptavidin-FITC (1/500 dilution) at room temperature for 1 hour and rinsed one more time. Next we did the nuclei staining with Hoechst (1/100 dilution) followed by mowiol mounting medium.

To solve the problems in tissue thickness in the Eriochrome C/Cresyl violet staining, in HA staining the problems also appear related to antibodies penetration in slices with 30 µm thickness. We did not achieve conclusive results and we changed the revelation step for HA staining using streptavidine-peroxydase and diaminobenzidine (Dako North America, Inc., Carpinteria, USA) rather than streptavidin-FITC. In the new protocol we add one step of immersion in hydrogen peroxyde 3% diluted in PBS, for 10 minutes, to block endogen peroxidase, next to 3 glycin baths. After that all the steps were maintained, adding the incubation for 1h at room temperature of streptavidin-peroxydase (dilution 1/200) after the overnight b-TGS6 (dilution 1/500) incubation, at 4ºC in a wet chamber, with a step of PBS rinsing between the two incubations. Finished the time of incubation of streptavidine-peroxydase, we made 3 washings in PBS and we add DAB to observe the colour change by timing time followed by blades immersion in distilled water to stop the reaction. Finally we counterstained nuclei with hemalun and we used DPX mounting medium.

Hyaluronan concentration (ELISA)

To quantify the hyaluronan present in sections of injured and uninjured spinal cords we used an HA-assay, very similar to an enzyme-linked immunosorbent assay (ELISA) but lacking capture and detection antibodies. The capture and detection system is based on the ability of HA to bind different HA binding proteins.

The first step was the lyophilisation procedure, frozen spinal cord segments of epicenter (E) and caudally (C+1) with 4 mm length, were weighted and underwent lyophilisation for 24 hours. Then dry samples were also weighted and then subjected to overnight digestion with 500 µL pronase 0.1 M per tube, with the aim to access hyaluronan. Next step was the pronase inactivation with tubes immersion for 15 minutes in boiling water, 100ºC. Next to cooling down the tubes to -80ºC, we did one second lyophilisation for 24h and we stored samples at -80ºC.

Measurement of HA concentration is most commonly determined by the use of a labelled specific HA binding protein, so we coated a 96-well microplate with 50 µL/well of capture reagent (composed by human recombinant aggrecan, CSPG), we incubated overnight at room temperature. Next day, we washed wells to remove the excess of capture proteins. We made the block buffer incubation step at room temperature for 1 hour.

Samples were resuspended in 100 µl distilled water per tube and standards were prepared using 90 ng/mL as the higher standard concentration, and doing a 3-fold serial dilutions we prepared standards concentrations of 30, 10, 3.33, 1.11 and 0.37 ng/mL, used to draw the six point standard curve.

We made a dilution of 1:1000 because HA was still highly concentrated in the lower tested dilutions of 1:10 and 1:100.

We added 100 µL to each well of samples and standards and we incubated 2 h at room temperature, allowing the fixation of HA to the HA-binding protein, aggrecan (a proteoglycan that combines with HA in the ECM, originating complexes).

We repeated the washing step previously done and we added the biotinylated HABP aggrecan, and we incubated 2 h at room temperature. Another wash step and the addition of streptavidine-horseradish-peroxidase (HRT), incubating at room temperature, avoiding direct light. A new wash step and next, peroxidase activity was assayed using sodium acetate buffer PH=6, as a substrate solution for the enzyme. After that we stopped the reaction and the colour appearance indicates the presence of HA, being the colour intensity proportional to the amount of enzyme present and thus to the HA concentration.

Optical density was determined at 405 nm and 570 nm on a microplate reader. We

subtracted readings at 450 nm and 570 nm, for correct the optical imperfections in the plate.

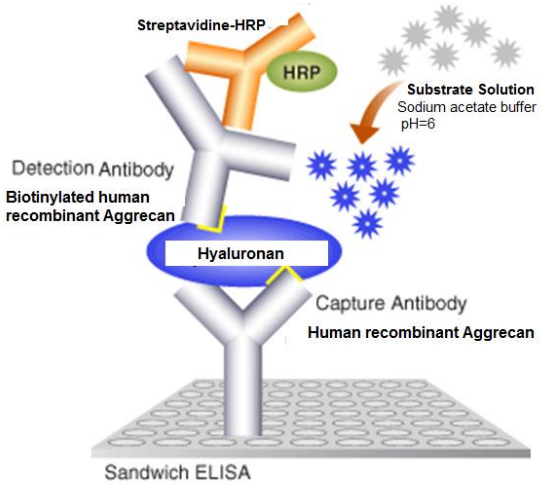

Figure 10: Elisa sandwich. Detection method used in HA dosage.

Quantitative real-time PCR

With the goal to access the alterations in expression of metabolizing HA enzymes (synthases and hyaluronidases) in the injured and uninjured spinal cords samples, mRNA expression was analysed using qPCR technique. Total RNA was extracted from the laminectomy and SCI groups using MagNA Lyser Green Beads (Roche), TRIzol® reagent (Invitrogen) and High Pure RNA tissue Kit (Roche), in which frozen (-80ºC) 29 samples were selected, between them the control organs: liver, skin and eye. Fourteen samples from laminectomy group and 12 samples from compression group. Epicenter (E) and more caudal (C+1) were the segments chosen for the RNA extraction.

Total RNA extraction

We began adding 1000 µL TRIzol® to each segment contained in the MagNA Lyser Green Beads tube, for the cells disruption and endogenous nucleases denaturing, preventing nucleic acid degradation. We homogenized samples in the MagNA Lyser Instrument. Next we recovered the supernatant and we added 200 µL of chloroform to each tube, incubating for 2-3 minutes at room temperature, resulting in the formation of 3 different phases: RNA (upper phase), proteins (interphase) and DNA (lower phase).
Next step was the transfer of 300 µL supernatant, without perturbing the interphase and the addition of 300 µL of ethanol 70% followed by centrifugation.

DNase was added to the tubes followed by 15 minutes of incubation at room temperature. This step prevented genomic DNA contamination.
Finally we added 500 µL of washing buffers and 100 µL of elution buffer included in High Pure RNA tissue Kit (Roche).
The quality and concentration, in ng/mL, were determined placing 2 µL of extracted RNA in the spectrophotometer reading (NanoDrop Technologies), at a wavelength of 260/280 nm. The ratio varied between 1.6 and 2.0. It was considered satisfactory for RNA purity.

Reverse transcription

Total RNA was reverse-transcribed into first-strand cDNA in a total volume of 20 µL using the SuperScript® III Reverse Transcriptase kit. RNA was diluted to a final concentration of the less concentrated sample, 14.56 ng/mL, with RNase free water, because all reactions must have the same amount of RNA. Then we added 2uL/sample from prepared MIX 1 (1 µL of dNTP mix, 0.1 µL poly-dT and 0.9 µL RNase free water) per sample. Reverse transcription included a first incubation stepat 65ºC, during 5 minutes. Next we added 7 µL from the prepared mix 2 (4 µL first strand buffer 5x, 2 µL DDT 0.1M 10x, 0.1 µL Reverse Transcriptase III and 0.9 µL RNase free water) and we submitted the tube to 42ºC incubation during 50 minutes and 15 minutes cooling. Finally we diluted 20X cDNA samples, preparing new tubes with 10 µL cDNA in 190 µL RNase water free.

qPCR reaction

For quantitative real-time PCR reaction volume of 20 µL, 5 µL of cDNA (concentration 14.56 ng/µL) from the RT-reaction was used as template, with 10 µL of SYBR™ Green master mix and 2.5 µL of 5' and 3' gene-specific primer at concentration of 300 nM/L each. Sequences of primers used for RT-PCR are shown in Table 2.
After the initial denaturation at 95ºC for 3 minutes, 40 cycles of primer annealing and elongation were conducted at 60ºC for 45 seconds, followed by denaturation at 95ºC for 10 seconds. Each cDNA sample was analysed in duplicate for mRNA of all genes. Thus, cDNA was amplified with Light Cycler ® 96 (Roche) RT-PCR system and quantified by the corresponding program (RT-PCR software Light Cycler ® 96 version 1.1.0.1320).
The RT-PCR was accompanied by the analysis of the dissociation curves.
Fluorescent emission data were captured and mRNA levels were quantified using the threshold cycle value (Ct).

For the analysis of gene expression, the $2^{-\Delta\Delta Ct}$ value was calculated where

$\Delta\Delta C_t = \Delta C_t$ - average of ΔC_t, where

ΔC_t = target gene C_t - average of housekeeping genes C_t (HPRT and beta actin)

Quantitative PCR data for mRNA of each sample were normalized by reference to the data obtained of the housekeeping genes HPRT and b-actine determined from the same sample.

Real-time PCR primers of HAS3 and Hyal2 genes, were synthesized by Eurogentec S.A. enterprise and designed by us using the Pubmed nucleotide database and Primer3 program version 0.4.0, according to the coding sequences of each gene and following quality criteria.

Table 2: Mouse primers pairs of HA related enzymes and housekeeping genes used in qPCR.

Genes of interest	Sequence 5'-3'
mHAS1 F	GCATGGGCTATGCTACCAAGTAT
mHAS1 R	AGGAGGGCGTCTCCGAGTA
mHAS2 F	GACCCTATGGTTGGAGGTGTTG
mHAS2 R	ACGCTGCTGAGGAAGGAGATC
mHAS3 F	CAGTGGACTACATCCAGGTGTG
mHAS3 R	CATCTCCTCCAACACCTCCTAC
mHyal1 F	CAGCATGCTCAGAAAGTTTGG
mHyal1 R	TGAGCAAGGTGGGTAACCAG
mHyal2 F	CGAGGACTCACGGGACTGA
mHyal2 R	GGCACTCTCACCGATGGTAGA
mHPRT F	GGCCTCTCGAAGTGTTGGAT
mHPRT R	CCAACAACAAACTTGTCTGGAA
mBeta-actin F	TCCTGAGCGCAAGTACTCTGT
mBeta-actin R	CTGATCCACATCTGCTGGAAG

Double-labelling immunofluorescence

Staining of tissues with 6 µm thickness of spinal cord waxed sections were dewaxed in toluene twice for 5 minutes followed by rinsing in alcohol, 3X for 1 minute and 10 minutes in tap water. Sections were then immersed in PBS for seconds followed by 3X during 2 minutes in Glycine 0.1M pH 7.2. Next, for sections permeabilization, saturation using PBS-0.2% BSA-0.02 %-Triton at room temperature for 1 hour was done.

Concerning primary antibody incubation, a monoclonal mouse anti-GFAP (dilution1:100) or a polyclonal rabbit anti-IBA1 (dilution 1:100) antibodies were used in combination with HA binding protein b-TGS6 (1:500).

Mixes of GFAP/HA and IBA1/HA were applied to the sections and slides were kept in a humidified chamber at 4ºC, overnight. Next day, the washing step in PBS-0.2%BSA-0.02%Triton was done and the incubation with the conjugated secondary antibody, goat α-mouse-Alexa 594 (dilution 1:100) or α-rabbit-Alexa 594 (dilution 1:100) or streptavidine-FITC, for 1 h at 4°C was performed. Another washing step PBS-0.2%BSA-0.02%-Triton were executed followed by counterstaining of all nuclei with Hoechst (dilution 1:100) in PBS-0.2%BSA-0.02%-Triton, during 15 minutes. All sections were coverslipped with mowiol mounting medium. Slides were imaged using a microscope Olympus BX-60®.

RESULTS

Setup of spinal cord compression model

Results showed that important visual lesions were done with injury percentages of 68% and 67% (Figure 11-C, D) in animals submitted to the longest compression time, 30 and 60 seconds. The differences between these two groups were reduced as the differences found between the other groups of 5 and 15 seconds of compression, which registered lower percentages of damaged tissue of 45% and 37%, respectively (Figure 11-A, B).

The lesions resulted from major compressing times achieved bigger lesion volumes, with an average volume of 3.03 mm^3 and 1.85 mm^3 for 30 seconds and 60 seconds of compression, respectively. The smaller lesion volumes of 1.27 and 1.23 mm^3 were reached by lower compression times of 5 and 15 seconds (Figure 12).

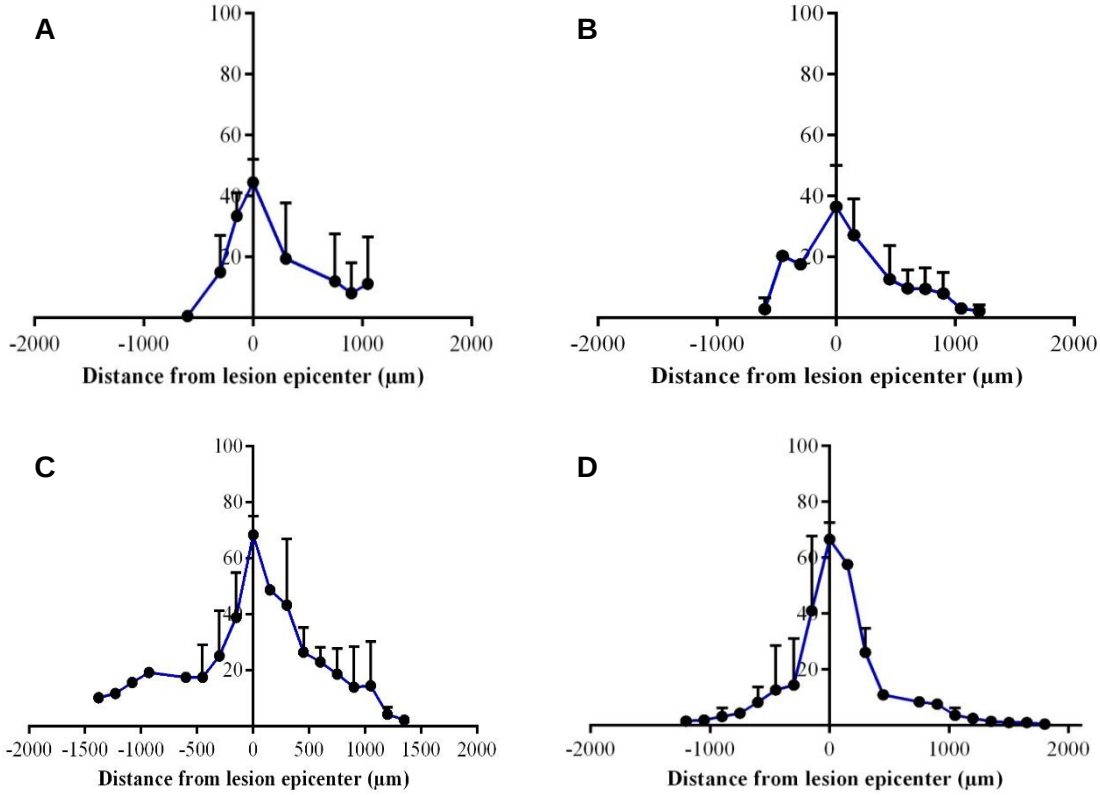

Figure 11: Lesion area measurements in Eriochrome C/Cresyl violet stained serial sections (30 µm thickness) from 2 mm rostral to 2 mm caudal from the injury site, spanning the entire injury site from animals subjected to four different compression times: 5 (A), 15 (B), 30 (C) and 60 seconds (D) at T9 vertebrae location. Y axis represent the percentage of damaged tissue measured by ImageJ software. The spinal cords were collected 2 weeks after injury and each graph represents 2 animals. Graph plot mean and error SD.

The lesion size results were expected, lesions were more extended with higher times of compression, registering values of 2.8 mm and 3.0 mm of extension of damage along the spinal cord while 5 and 15 seconds achieved little extensions of 1.7 mm and 2.0 mm, respectively (Figure 13).

For all next experiments, we chose 30 seconds of spinal cord compression as the suited compression time was chosen because this duration was sufficient to cause moderate damage, with the suited match for the results of damaged area, volume and extend of injury, resulting in the expected phenotype of bilateral paraplegia.

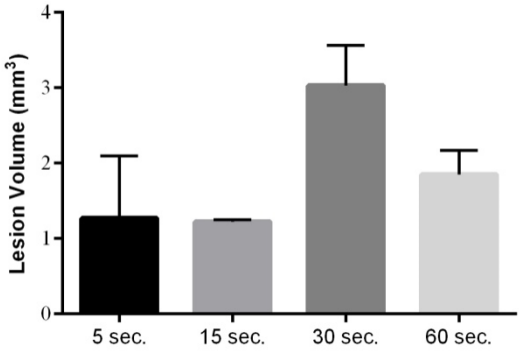

Figure 12: Lesion volumes (mm3) generated by different times of compression. Quantitative lesion analyses show differences for the lesion volume created in 4 different groups. Graph plot mean and error SD, n= 2 animals per group.

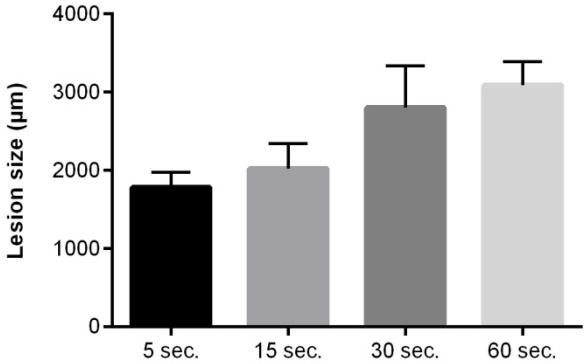

Figure 13: Rostro-caudal extension of the lesion along the spinal cord, in micrometers (µm), caused by the different compression times tested in this study. Results show differences among the groups with lower and higher compression times. Graph plot mean and error SD, n= 2 animals per group.

Epicenter as the more injured area

Observing the stained Eriochrome C/Cresyl Violet sections, we saw samples from laminectomy (control group) presenting a normal tissue architecture with clear delimitation between gray and white matter (Figure14-A).

In SCI group, there was histological alterations, like the disruption of tissue architecture at the site of damage and around them and the boundary between the white and grey matter was not evident (Figure 15-A).

Beyond that, the cell population present in laminectomy group was unchanged, with normal cellularity in both grey and white matter (Figure 14-B).

At two weeks after injury, high cell density (Figure 15-B) and cavitations were evident in injured spinal cords. These alterations were present in both white and grey mater areas, mainly in the grey matter of the ventral part of the spinal cord.

The epicenter was the region where the greatest damage has been observed showing structural disorganization with an extent of tissue damaged that tapered with increasing distance rostral and caudal to the lesion epicenter.

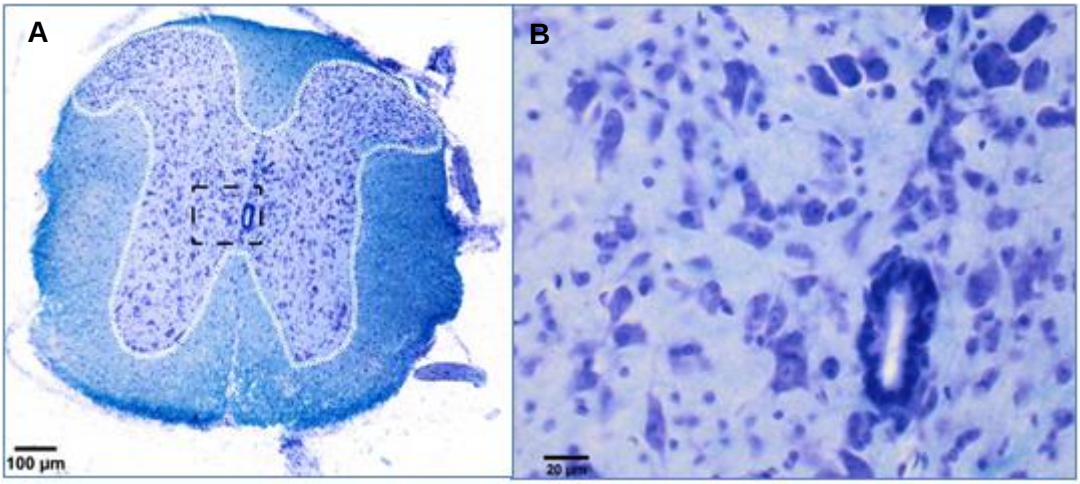

Figure 14: Cross-sections stained with Eriochrome C/Cresyl violet with white matter in blue and in violet all the nuclei and Nissl's bloc present in both grey and white matter. **A**- Control group, Laminectomy showed normal cytoarchitecture with clear delimitation between WM and GM (white dotted lines). **B**- Magnification 40 times of GM region showed in A, showing normal cellularity and an intact central canal surrounded by ependymal cells, in the center. Scale bars represent 100 µm (A) and 20 µm (B).

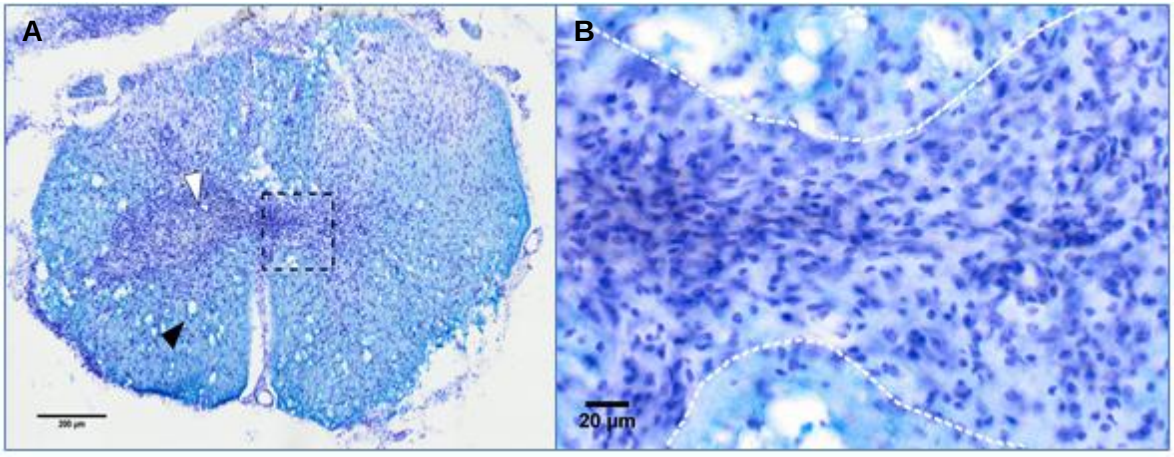

Figure 15: Sections of the lesion epicenter in animals subjected to compression of the spinal cord, showing the disorganisation post-SCI between WM and GM regions. **A** - Presence of degraded tissue more evident in white matter but also present in grey matter represented by arrow heads, in black and white, respectively. Dotted black square denotes the gliosis region magnified in B.
B - High glial cell density in grey matter corresponding to the process of astrogliosis and formation of the glial scar represented between dotted lines. Scale bars represent 200 µm and 20 µm.

Progression of grey and white matter damage

After trauma, grey and white matter injuries advance differently along the spinal cord. Observing GM we see visibly uninjured GM tissue from 0.5 mm, to both sides of the centre of the lesion, in animals subjected to 30 seconds of compression.

In WM the important part of the injury was situated along 1 mm from lesion epicenter, to both sides of the spinal cord (Figure 16-D). However, beyond 1 mm of lesion extension, we still verified some sporadic morphological abnormalities (Figure 16-B).

Results show that injury caused to GM is localized around epicenter, along short distances (Figure 16-C), evidencing complete tissue disorganisation, cellular proliferation and cavitations (Figure 16-A).

Injuries to white matter tissue were generally characterized by the appearance of multiple cavities in the tissue, both epicentre sides, resulting from macrophages action in cleaning the damaged tissue and cellular debris.

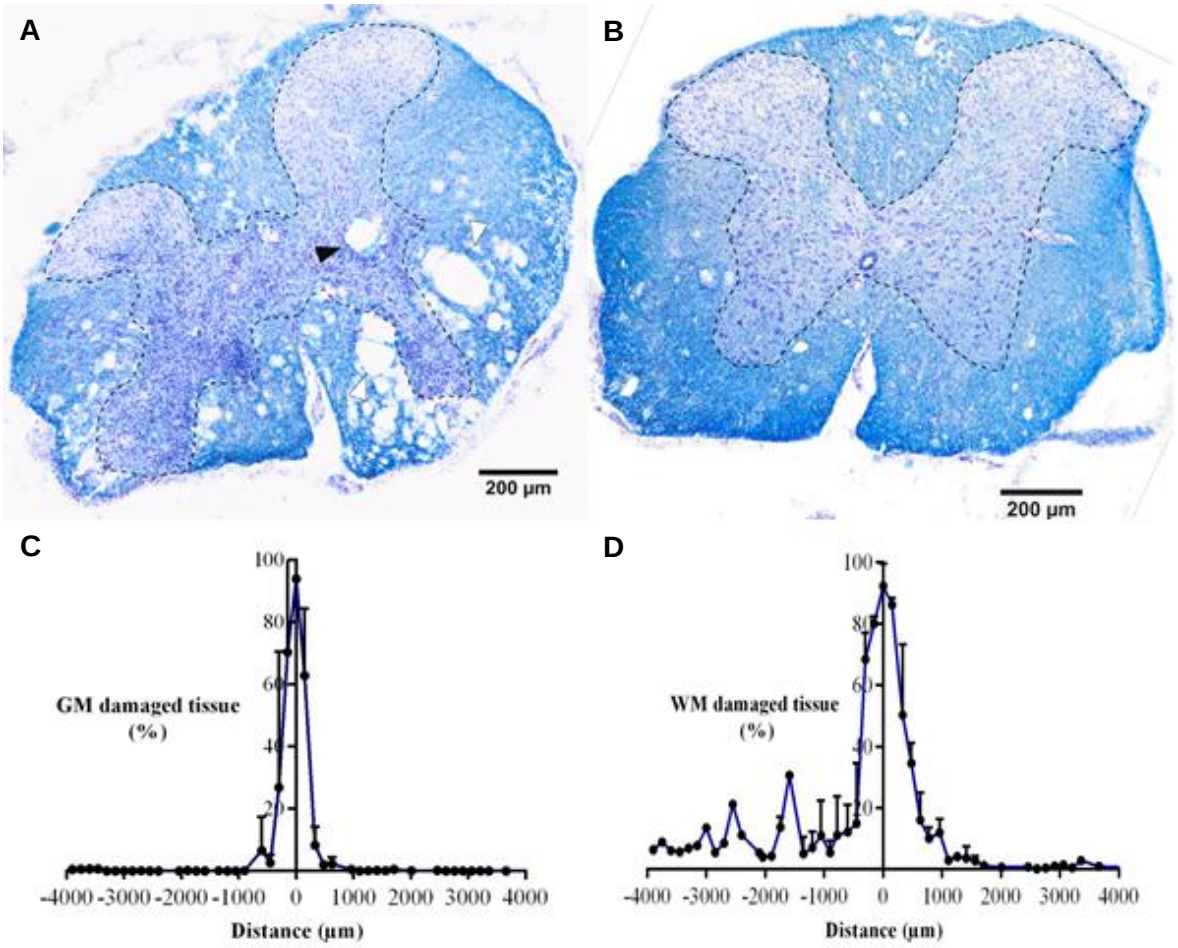

Figure 16: Quantitative and histological findings show the lesion extention in GM and WM **A**- At 300µm in caudal (C) direction, both grey (black arrow head) and white matter (white arrow heads) were damaged. More important damages were located near the epicenter. **B**- WM damage extends for longer distances, and at 780µm more caudal (C+1), grey matter is unaffected, contrary to white matter that keeps the vacuolisation despite it being less significant. Graphs show results of damaged tissue measurement from Eriochrome C/Cresyl violet stained sections along 4 mm fom lesion epicenter to both sides. The amount of injured WM was observed from a bigger extension (**D**) than GM injured tissue (**C**). Scale bars represent 200 µm. Graphs plot mean and error SD, n=3

Motor neuron counts

Eriochrome C/Cresyl violet stained sections were analysed for total counts of large ventral horn motor neurons at 2 weeks post-injury. Mice receiving thoracic compression showed loss of ventral horn motor neurons at multiple distances around the lesion epicenter.

Knowing that uninjured mice has got between 20-30 motor neurons, our results showed a decrease in the number of motor neurons in ventral horn, reaching the lowest value at the epicenter, with no motor neuron counted. More important loss happened during more than 1 mm for each side of the site of injury (Figure 17).

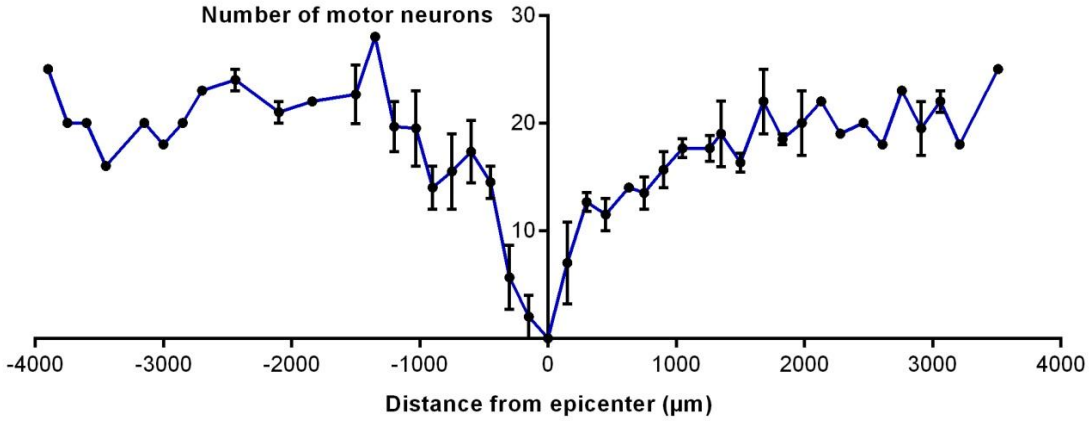

Figure 17: Quantification of total thoracic motor neuron loss. Motor neurons were identified on Eriochrome C/Cresyl violet sections and were manually counted in both ventral horns following T9 injury. There is an important loss of motor neurons along more than 1 mm from lesion epicenter. Graph plot mean and error SEM, n=3.

Behavioural assessment in injured mice

Animals were scored in the different tests before the surgery and the BMS score of 9 was registered for all animals of the two groups involved in this study.

After the operation all animals were graded over again and the laminectomy group showed no obvious deficits after recovery from anaesthesia, exhibiting normal locomotion. However in the group submitted to compression of the spinal cord, mice showed loss of motor function with decreased physical ability in the hind limb movement. They had flaccid paralysis and maintained this pattern at 3 days post-surgery (BMS=0). But mice did not respond by the same manner to injury and there were animals with this phenotype until 9-10 days post-injury.

During the first week post-injury, half part of the animals recovered the extensive ankle movement (with a group average BMS=2) and afterwards showed improvement until stepping. During the first two weeks, the group demonstrated frequent dorsal stepping (BMS score=3) or occasional plantar stepping (BMS=4) but without coordination, contrary to some animals in the same group that at this time course reached stepping with hind limb-forelimb coordination (BMS=5-6).

Despite the rapid and progressive recovery, animals never recovered totally their motor function after 6 weeks. At this time, most of them improved to the late phase of recovering (BMS score 5-8) but only one mouse achieved the maximal score of 9 that corresponds to normal locomotor mobility, with trunk stability and refined performance. Similar to Basso *et al*., 2006 along the observations distinct behaviours that indicate trunk instability, such

extensor spasm with the full extension of knee and ankle joints, flexor spasm, in which the hindlimb is sustained in a flexed position and does not step, or lateral displacement of the trunk were found.

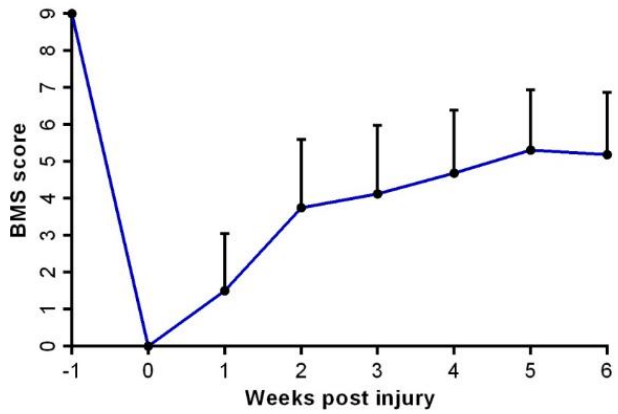

Figure 18: Line graph representing Basso Mouse Scale score (BMS score) of SCI group. Results measured daily represent an average of the animal group (n=16). Before injury to spinal cord (x=-1), all animals had the higher BMS score of 9, but after the SCI, the score dropped to 0, which maintains until day 3 for all animals. During the recovery time they were not able to obtain the same performance before surgery. Error bars represent SD.

Grip strength and hanging wire tests showed that injury to the spinal cord is associated with reduction in muscles strength. In grip strength, results show that mice improved the strength exert on the grid to the maximum average group of 49.5 g but they didn't recover the initial performance of the group achieved before the surgery, 75.3g, even 6 weeks post-injury. Grip strength test results represent the specific force of mice hindlimbs exerted on the grid (Figure 19).

In hanging wire test the decrease of ability to execute the test was not so felt due to the fact that in this test animals may also use the forelegs to remain attached to the grid when the cylinder was returned (Figure 20-A). However we can see that also in hanging wire test, their physical abilities were reduced, with the decreased muscle strength confirmed by grip strength results.

In Rotarod test, mice registered the worst performances post-injury of all behavioural testes, giving us important informations about loss of motor coordination and cerebellar dysfunction probably resulting from the spinocerebellar tracts disruption.

Figure 19: Time course of grip strength test showing an alteration in hindlimbs animal strength after traumatic spinal cord injury. Each point represent the group average. Error bars represent SD, n=13.

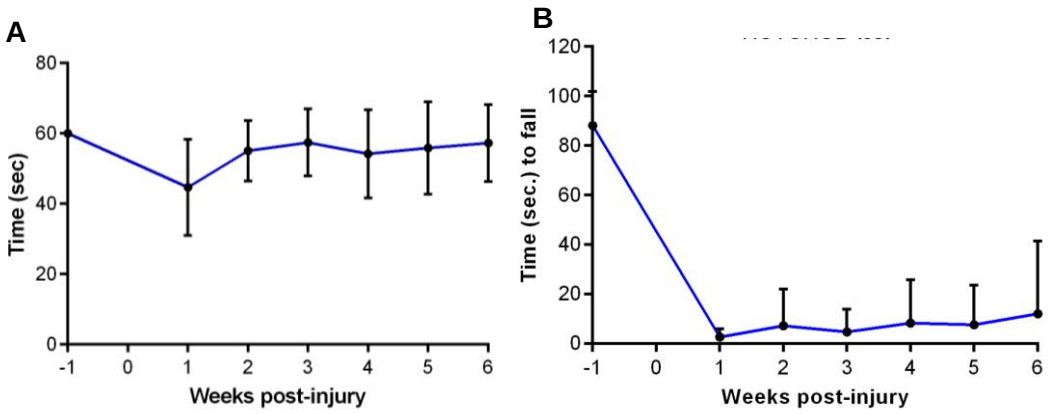

Figure 20: Time course of hanging wire (A) and rotarod (B) tests performance after SCI of mice. Each point represent the group average (n=13 and n=16, respectively), error bars represent SD.

Hyaluronic Acid localization in spinal cord

Observing the images for HA staining, we see presence of HA in the spinal cord sections of control animals (laminectomy group), mostly in grey matter area, forming the condensed perineuronal nets around neuron cell bodies (Figure 22-A), and radial striations of HA (Figure 22-B) are present also in white matter, along neuritis (dendrites and axons).

But at two weeks post injury, injured animals (compression group) show empty areas in lesion epicenter, suggesting the absence of HA at this location, mainly in the center of the spinal cord sections (grey matter).

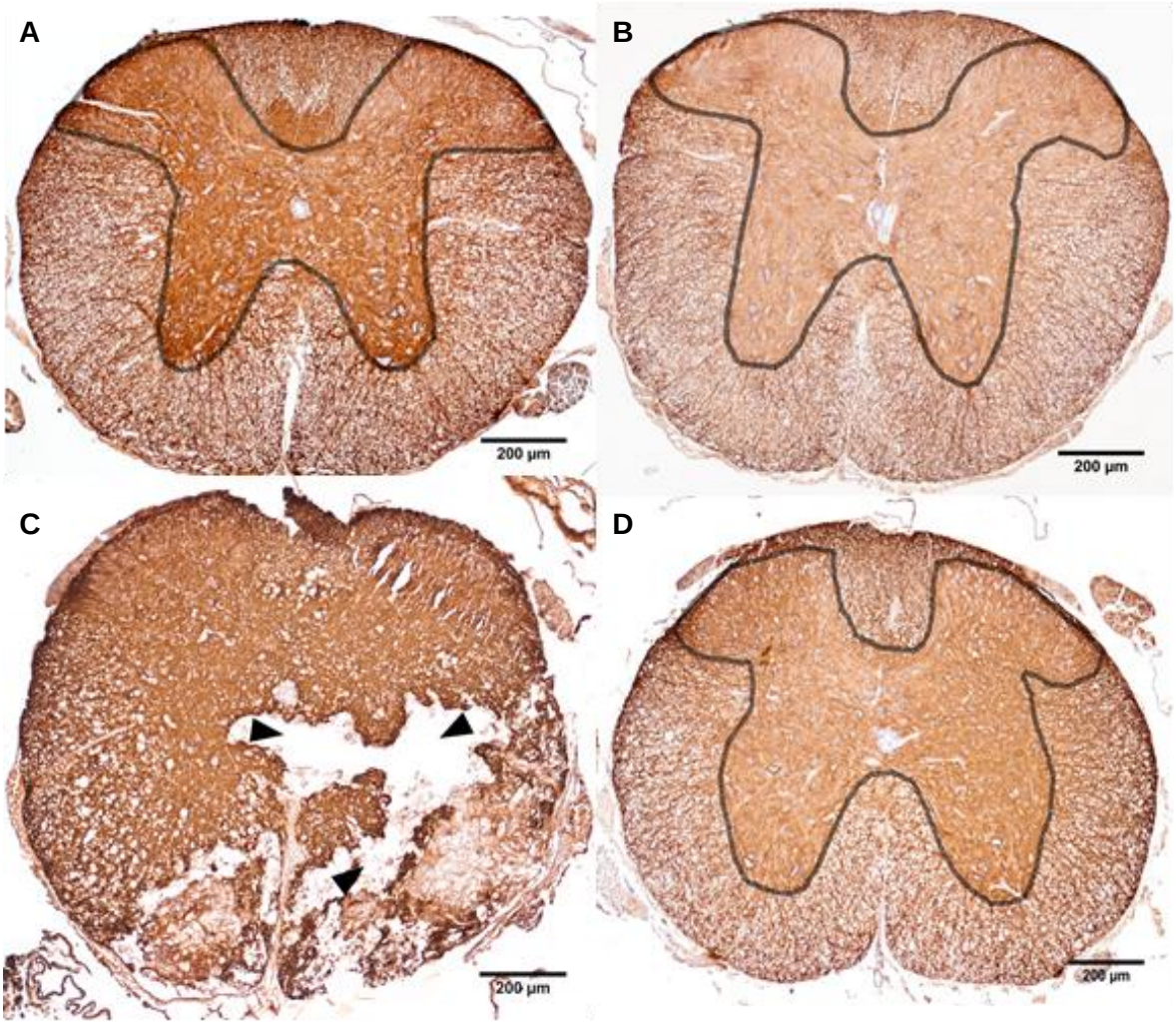

Figure 21: HA staining with streptavidine-peroxydase and revelation with DAB, in laminectomy epicenter (A), laminectomy caudal (B) compression epicenter (C) and compression caudal (D). In both groups, the epicenter T9 sections seems to be more intense stained than sections localized caudally to the lesion. Although, after injury, HA localization was disturbed at the epicenter, revealing areas completely devoided of HA, delineated with strong HA immunoreactivity at the boundaries, between intact and injured tissue. Scale bars represent 200 µm.

It seems that epicenter region, in both, laminectomy and compression groups have high density of HA binding sites for bTGS-6 than regions situated more caudal or rostral from epicenter.

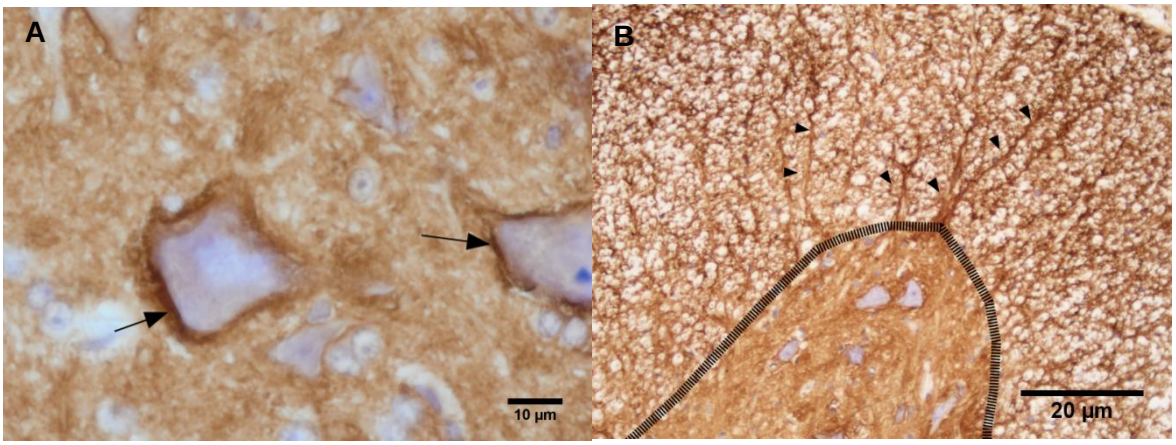

Figure 22: HA is present in a condensed way around neuron cell bodies (PNN) (**A**) and along proximal dendrites (**B**). Scale bars represent 10 and 20µm.

To execute and obtain these results human skin (**A**) as positive control was used and as negative controls mouse skin (not shown), human skin (**B**) and spinal cord incubated with PBS-0.2% BSA- 0.02% rather than the primary antibody b-TGS6 (**C**) were used.

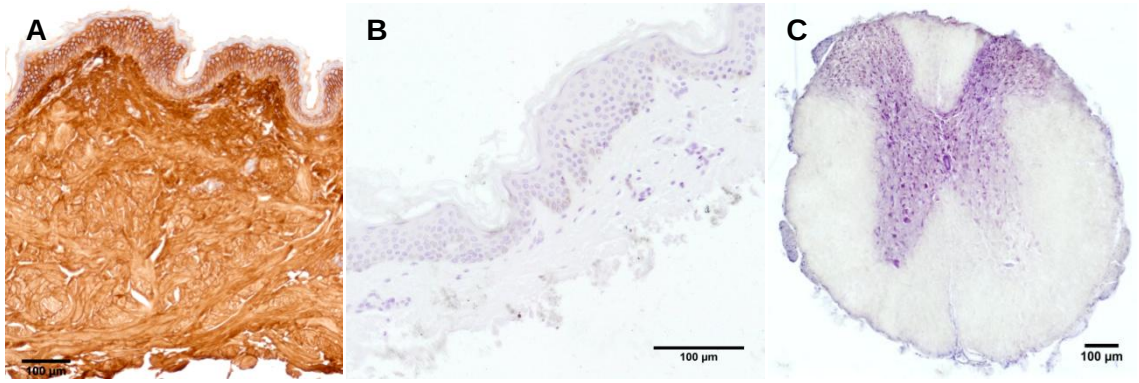

Figure 23: Images represent positive control, human skin included in paraffin (A) and negative controls, human skin (B) and spinal cord section (C) used in the HA staining experiment. Scale bars represent 100 µm.

Double-labelling Immunofluorescence

To determine which cellular population is responsible for HA production, or at least co-localize with HA-expressing spinal regions, we determined whether HA/GFAP or HA/IBA 1 were co-expressed in laminectomy and compressed spinal cord using a double immunofluorescence experiment.

Completely different results were obtained to controls and injured mice, at two weeks post-injury.

In control animals, in green, the presence of HA in grey and white matter was seen. In

GM, HA immunofluorescence was more condensed, like in HA staining experiments, being visible the perineuronal nets (PNNs) around neurons cell bodies, once again (Figure 24-A). These animals didn't show signs of co-localization for HA/GFAP^{+} and HA/IBA 1^{+} cells in both white and grey matter areas (Figure 24-C, D).

In fact, quiescent astrocytes are GFAP^{-} and no microglia could be observed in uninjured animals.

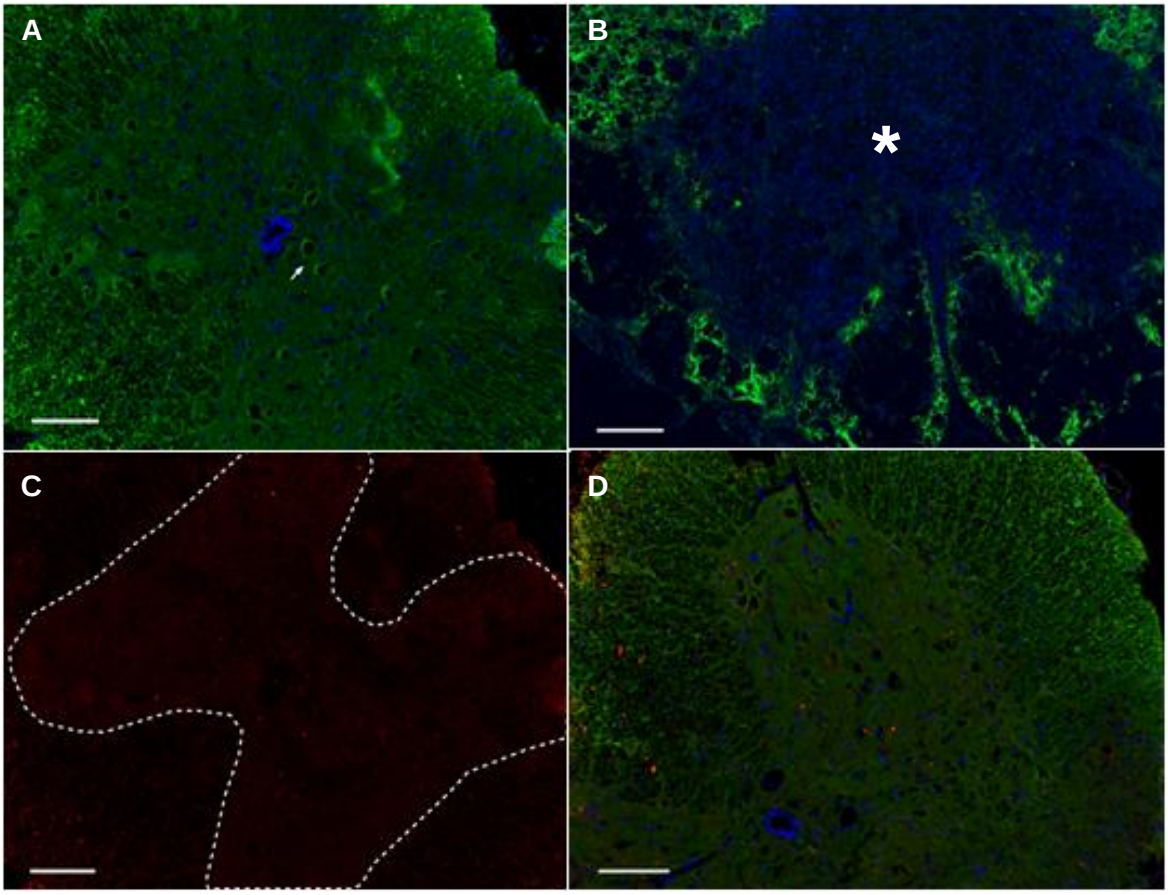

Figure 24: Distribution of HA is altered after mouse spinal cord compression injury. Photomicrographs of cross sections of spinal cord after laminectomy (A) and compression (B) to the T9 vertebrae labelled for HA. Sections (6 µm) were labelled with biotinylated HABP (b-TGS6 and detected with a fusion molecule streptavidin-FITC (green) combined with antibodies against GFAP (to label astrocytes) or IBA 1 (for microglia cells). **B**- HA expression is decreased dramatically in lesion epicenter, at 15 days after mouse spinal cord compression injury. **C,D**- In uninjured spinal cord (laminectomy) expression of IBA 1 (red staining-C) and GFAP (red staining-D) is very low. Cells were counterstained with Hoechst (blue staining) to detect nuclei. Asterix in B depicts the lesion core. Scale bar = 100 µm.

In injured animals, two weeks post SCI, we saw the up regulation of GFAP and IBA 1 co-localized with HA. Co-localization of HA/GFAP^{+} was seen in white and grey matters, being more relevant in grey matter (Figure 25-D) of the sections adjacent to the lesion core.

Co-localization of HA/IBA1^{+}, were less evident and also mostly present in grey matter

tissue (Figure 25-A).

Contrary to the control group, after two weeks of trauma, we confirm the absence of HA in the lesion center, as we observed with HA staining, being only located in a more concentrated manner at the boundaries between intact and injured tissue (Figure 24-B). High cell density stained in blue by Hoechst and any green fluorescence were recorded at the centre of the lesion (Figure 24-B). However, around the empty epicenter we also had the opportunity to see the appearance of some positive GFAP cells in the beginning of the process of the glial scar formation (Figure 25-C).

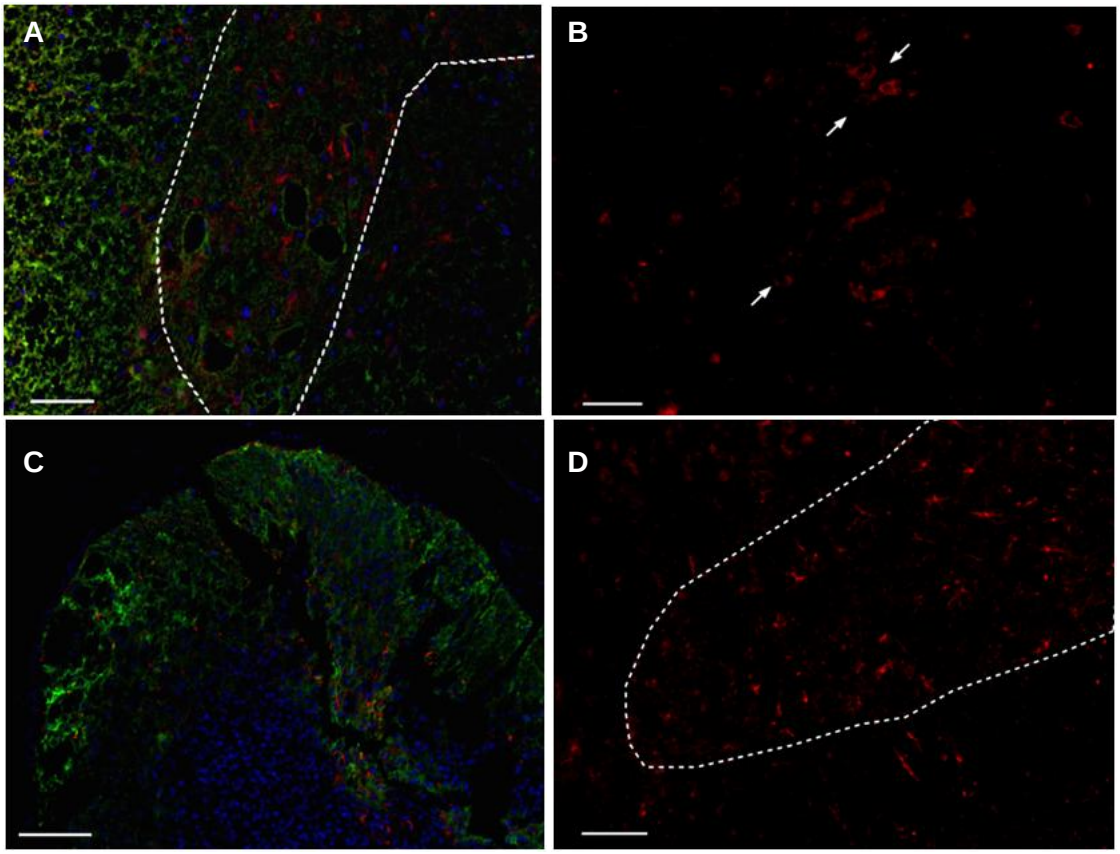

Figure 25: immunofluorescence double-labelling for HA/IBA1^{+} (A) and HA/GFAP^{+} (C). Results of HA/IBA1^{+} reveal up-regulation of IBA1 after spinal cord compression injury. **A**- Photomicrograph of ventral horn of injured spinal cord sections showing high presence of IBA 1 positive cells in grey matter. **B**- Magnification 40X of the up regulated microglia cells. HA/GFAP expression is also up regulated after spinal cord mouse compression, high expression of GFAP in ventral horn of an injured spinal cord is visible in red (C). Lesion epicenter is surrounded by GFAP positive cells represented in higher magnification in D. Scale bars = 50 µm (A, C) 20 µm (B) and 100 µm (D).

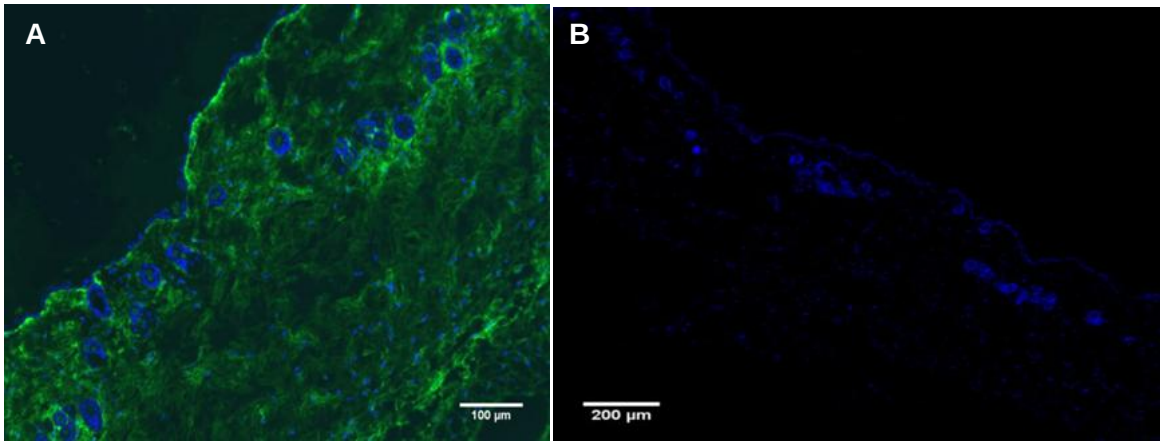

Figure 26: Controls used in double-immunofluorescent technique. **A**- Mouse skin as positive control, 10X magnification. **B**- Mouse skin as negative control, 4X magnification. Scale bars represent 100 and 200 µm.

Differential expression of HA metabolizing enzymes

Fold change in mRNA expression between the control animals (laminectomy) and animals subject to spinal cord compression was calculated using the qPCR equation:

$$\textbf{Fold change} = 2^{-\Delta\Delta Ct}$$

T student test didn't showed significant effect of compression injury to the spinal cord on mRNA expression of synthases (HAS1, 2 and 3) and hyaluronidases (HYAL1 and HYAL2), two weeks after injury. Mann-Whitney test (two tailed) showed that compared to control animals (laminectomy), HAS1, HAS2 and HAS3 mRNA expression did not change in injured animals, 2 weeks after SCI, (p=0.057, p=0.2 and p=0.742), although there is a trend for decreased of HAS1 expression.

In this first expression analysis only the epicenter segment was included for both groups (Figure 27-A, B).

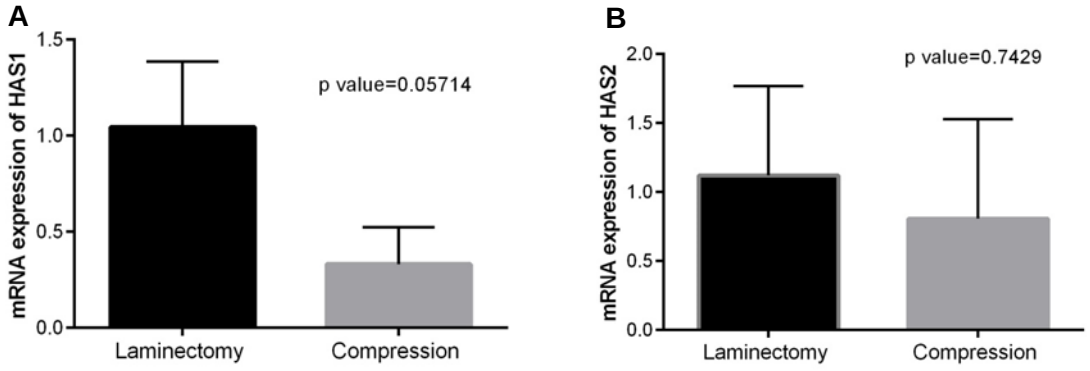

Figure 27: Quantitative real-time PCR determination of HAS 1 (A), HAS 2 (B) mRNA expression in the epicenter of laminectomy and mice submitted to spinal cord compression, at 2 weeks post-injury (n=4 and n=3) p=0.057, p=0.7429.

About HAS3 expression we see the increased expression in all tested regions of the injured spinal cord, with the epicenter achieving 3.7 fold more HAS3 expression than laminectomy epicenter.

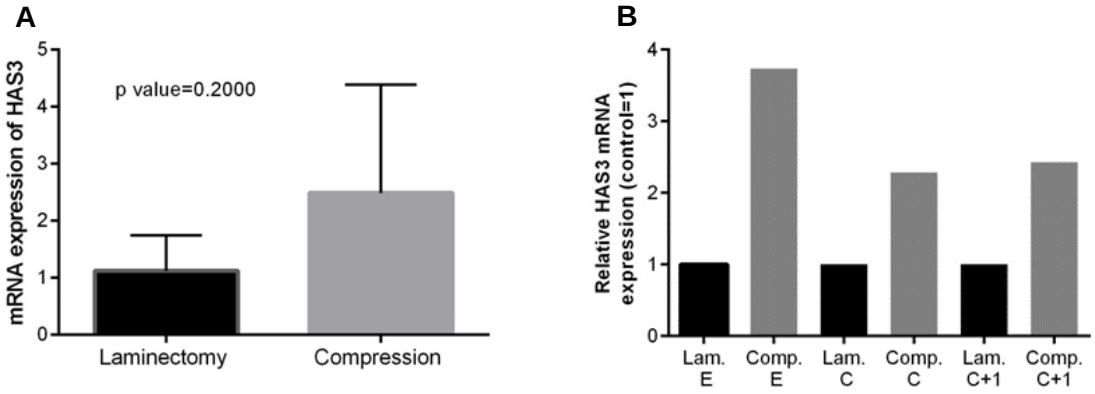

Figure 28: In injury, there are an increase in HAS3 mRNA expression compared with laminectomy group. A- In compressed spinal cord, mRNA of HAS3 is expressed more than two fold when compared with laminectomy group. B- mRNA HAS3 expression is up regulated in all regions, post injury, being the higher expression at the epicenter region.

Differences between injured and uninjured animals was more relevant for hyaluronidases (HYAL 1,2). In a general way, both hyaluronidases show higher expression before injury, but HYAL1 seems to increase his expression along the spinal cord while HYAL2 is higher beyond the epicenter, in regions more caudally (Figure 29).

No significant effect of compression in injured animals for HYAL 1,2 mRNA expression level was found (p=0.4 and p=0.7, respectively).

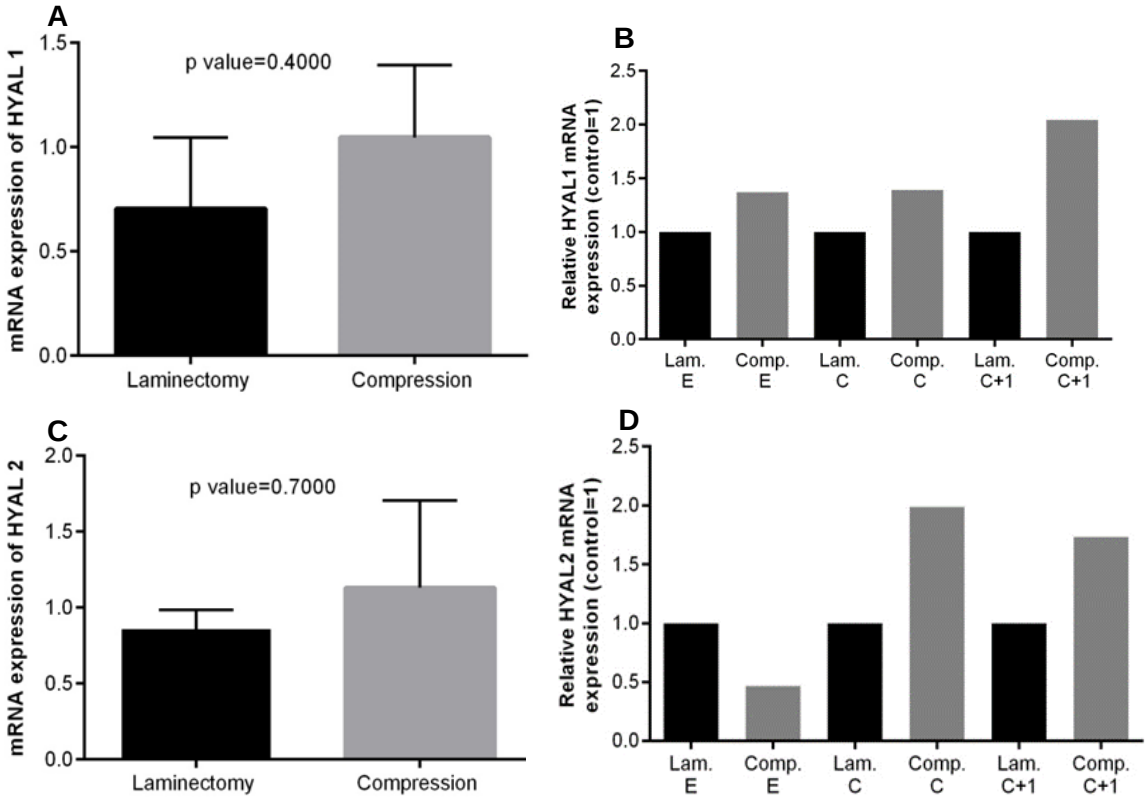

Figure 29: Quantitative real-time PCR determination for HYAL1 (A), HYAL2 (C) mRNA expression. B, D- is shown the relative Hyal1 and Hyal2 mRNA expression specifically in segments of the epicentre (E), caudally (C) and more caudally (C+1) of mice spinal cord compression (Comp.) and laminectomy (Lam.) at 2 weeks post-injury. Results are presented as the fold change relative to the control group (=1). (n=5 and n=4).

For the quantification of fold changes, we used always the arithmetic average of the two housekeepings genes, b-actin and HPRT, but first we saw the correlation between these two genes to know if we had a pattern of expression.

Results show a strong correlation between both housekeeping genes (HPRT and b-actin). So was decided to use the arithmetic average of these genes for the q-PCR normalization, because sometimes it requires the use of multiple reference genes to ensure accurate results, however, these genes has been appointed as the housekeeping genes commonly used that despite being expressed in all tissues, their expression level is not constant across tissues, varying considerably under different experimental conditions and therefore their use for normalization is limited (De Jonge *et al*., 2007).

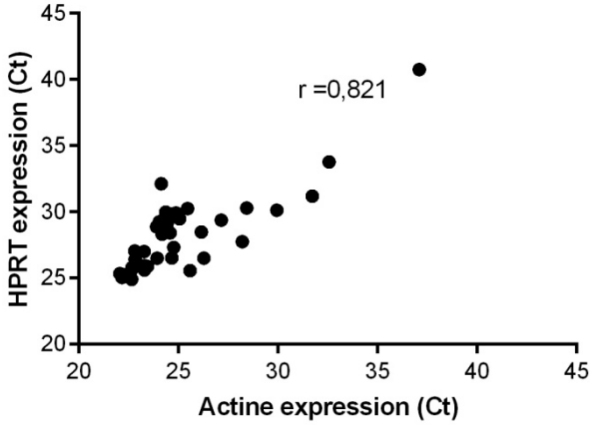

Figure 30: Correlation (Pearson) between the housekeeping genes used in qPCR normalization: b-actin and HPRT for several independent samples. Results are expressed as Ct, as the cycle number at which the fluorescence generated by the housekeeping genes in the reaction crosses the fluorescence threshold, the fluorescent signal significantly above the background fluorescence. The threshold cycle is inversely proportional to the original relative expression level of the gene of interest. In the graph we see that the housekeeping genes are expressed at a similar level. Results showed a positive correlation with a correlation coefficient of r=0,821

Hyaluronan concentration (ELISA)

Estimation of the HA concentration depends upon the construction of a standard curve.

The standard curve (Figure 31) was traced after collecting the absorbance results achieved for each standard. The concentration of the unknown samples was determined by interpolation which relies in the equation generated: $y=10.031x^2+0.5795x+0.2742$.

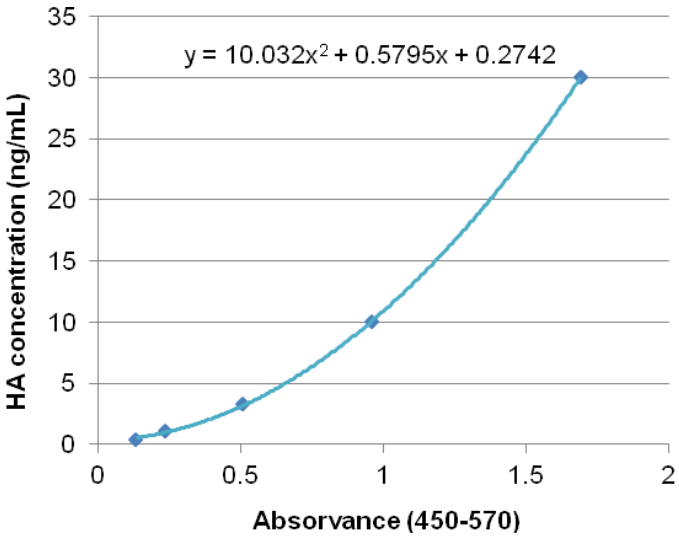

Figure 31: Standard curve of HA absorbance, constructed from the absorbance reading from standards of 30, 10, 3.3, 1.1 and 0.37 ng/mL concentration used in the experiment. Absorbance values were obtained for 3-fold serial dilutions in reagent diluent (5% Tween 20 in PBS, pH 7.2-7.4, 0.2 um filtered). The equation generated was y=10.031x2+0.5795x+0.2742.

Comparing the two groups of mice (uninjured versus injured), HA concentration in the spinal cord didn't change dramatically with injury or laminectomy. The epicenter region has the higher hyaluronan concentration in both groups, compression group had the same level in laminectomy group, with 2767.7 and 2732.8 ng/mL of HA, respectively.

However caudally to lesion epicenter the HA concentration was lower, and difference between two groups of mice were more pronounced, laminectomy group obtained 1324.3 ng/mL of HA and a decreased quantity in compressed spinal cord, registering 1034.8 ng/mL.

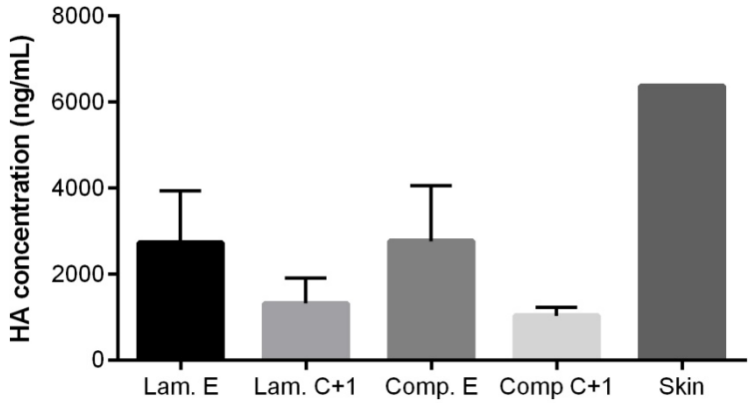

Figure 32: Analysis of HA concentration (ng/mL) in two different locations of the spinal cord, epicenter (E) and more caudal (C+1), of control animals (Laminectomy) and SCI animals (compression) by ELISA assay. Error bars represent SD, n=5 and n=4.

Discussion of results

Reversing paralysis that occur following SCI, is one of the big challenges in neuroscience research. Despite the significant improvements in understanding the SCI pathophysiology and in rehabilitation management, there are no treatment to improve neurological outcomes after SCI.

Several experimental models have been developed to simulate spinal cord injury and reproduce it in homogeneous form, in order to analyse the locomotor function response (Marques *et al*., 2009 and Kundi *et al*., 2013).

Our spinal cord injury model reproduced histological and functional changes very similar to human SCI.

In our model the primary injury is caused by the forceps impacting on spinal cord tissue, disrupting the structure and causing haemorrhage, often visible bruising of the spinal cord, followed by compression causing temporary tissue displacement and ischemia.

For this experiment we choose 30 seconds of compression as the suited time to obtain bilateral hind limb paralysis with flaccid limbs and no response to removal the paws when pinching. Bladder function was also compromised. Such aspects are related to the type of injury-induced characteristic in the model produced in this study.

Through the performed behavioural tests we could assess and evaluate the changes in motor function, such as locomotion, balance/coordination of forelimbs-hindlimbs and muscle strength, caused by injury.

The animals had their best personal score in all behavioural tests before surgery, then this score falls to 0 at the time of injury with progressive recovery along the 6 weeks follow-up but without reaching pre-injury score. Immediately after injury we observed decrease motor ability performing the same tests, however over time, spontaneous mechanism of recovery present in mice gradually improved the reminiscent motor function in locomotion and muscle strength along 6 weeks, despite the period of time not being enough to obtain complete recovery with same scores measured before.

Our behavioural results at two weeks are related with the neuronal damage observed in histological sections at this time course, because we had an important disruption of the gray matter with increased proliferation of glial cells, astrogliosis, mainly in lesion epicenter and in white matter, we had tissue vacuolization that extends rostrally and caudally from the lesion epicenter. Loss of motor neurons also correlates with decrease ability to mice hind limb locomotion.

The establishment of the injury model allowed us to verify HA presence in normal and

damaged spinal cord through HA staining. HA was present, although in a different way, in laminectomy group and in injured group. In normal spinal cord, hyaluronan was distributed homogenously in the grey mater, more concentrated at the PNNs and along the radial tracts in the white matter.

After SCI, the HA deposits were absent in lesion core and present at the boundaries suggesting the downregulation of HA matrix from the impact site, and an upregulation around the lesion core most likely synthesized by reactive astrocytes

The absence of HA in the lesion core were saw also in double immunohistochemistry, with the presence of infiltrating cells at the impact site and higher number of $GFAP^+$ cells that begin to appear around the empty central lesion.

With the aim to know more about HA synthesis and degradation, we analysed the expression level of HA metabolizing enzymes.

The balance between HA accumulation and degradation lead us to a better understanding of HA metabolism that is crucial in influencing cell behaviours, such as proliferation of astrocytes (Struve *et al*., 2005) or differentiation of NSPC cells (Sherman *et al.,* 2015)

Results of gene expression for HA-related enzymes were not significant in any of the cases, highlighting only the trend of HAS1 to decrease after insult to the spinal cord in a way almost significance, but results must be confirmed using a higher number of animals.

However there are a differential expression pattern for the HA metabolizing enzymes after SCI that seems to be altered in respond to damage and can work as a regulation mechanism of healing.

We were interested in checking the amount of HA present after damage, relating to the amount of HA in the control group. However, at two weeks after injury, similar HA concentration were measured in the epicenter of both groups and a slight decrease in HA concentration, caudally to the lesion core of damaged animals. Generally, after insult to the spinal cord HA concentration in epicenter doesn't change and more caudally the change was not dramatic.

But result becomes understandable when we know that from a published rat spinal cord injury, dramatic HA degradation occurred at the site of injury and in adjacent tissues, as early as 3 days post injury, but in following days HA amount is subsequently elevated being accumulated between 5 days and one month after injury (Struve *et al*., 2005). In fact, accumulation of hyaluronan is a hallmark in damaged CNS from ischemic injuries, seizures, traumatic brain injury, demyelinating diseases and normal aging, persisting for long periods of time after the initial insult (Sherman *et al*., 2015).

Given that we were not able to evidence any significant changes in HA amount and in

gene expression for HA-related enzymes between uninjured and injured animals, we performed immunohistochemistry against HA and double immunofluorescence to visualize HA location in the spinal cord and its potential re-localization after SCI. Results confirmed the presence of HA likely by astrocytes, visualized by co-localization of $GFAP^+$ cells and biotinylated-HABP, mostly in grey matter.

Post-injury, microglia and macrophages are also present in lesion, to a lesser extent than $GFAP^+$ astrocytes but once again mostly in grey matter, proven by presence of IBA 1^+ cells. We suspect about HA production from microglia although the co-localization of IBA1+ cells and biotinylated HA not being so obvious.

Macrophages and microglia, in grey matter of damaged animals exhibited an activated phenotype with cellular hypertrophy and retraction of cytoplasmic processes.

Our study provides preliminary molecular evidence of altered gene expression for HA-metabolizing enzymes in mouse spinal cord compression model.

Further study of HA metabolism, and understanding how expression changes along the time course could help us to better understand the role of HA in the healing process after SCI.

Limitations of the study

Deciding how large an experiment needs to be is a critical point of interest because the importance of the ethical implications that press and restrict increasingly the animal use in research.

The experiment can't be too small risking to lose biologically important effects, but also cannot be too large to protect animals from the unnecessary or inappropriate use.

In our study, concerning morphological analysis the population is too small to analyse statistically, being a limitation of our study.

Relating to mRNA expression level for HAS 1-3 and Hyal 1-2 HA metabolizing enzymes, we didn't validate our results, protein level were not determined due to the lack of suitable specific antibodies for HA needed to performed western blot analysis.

Further study is necessary to determine whether HA metabolism (synthesis and degradation) is associated with recovery of mice from SCI.

It would be interesting to characterize the molecular weight of HA synthesized post-injury, through the size-exclusion chromatography. This is a point of importance due to the different biological activities of different HA lengths described in the literature.

Mice models give us the advantage to produce mice with specific deletion of targeted genes (knockouts), so it would be interesting to check the HA concentration at the lesion epicenter and consequent behavioural results for hyal1 knockout mice.

Through the cell cultures with astrocytes, microglial cells and neurons will be interesting to confirm which cells produce HA after injury of the spinal cord and if the HA presence confer benefits on re-permeabilization of the glial scar, it would be interesting to promote HA secretion from the appropriate cell group modulating the synthesis rate or degradation rate of HA.

Limitations in reaching more results

Animal models are irreplaceable to understand the pathophysiological knowledge on cell injury, the evolution of damage and repair process of spinal cord needed for the development and evaluation of therapies for SCI.

But investigations with animal models require beyond the knowledge of the ethical standards and animal care, requires time. Time to reproduce the experimental SCI that require training, it is necessary time to breed and to care animals, inspect regularly wound healing, weight loss, dehydration, infection and any discomfort.

In the first experiments, we had some infected mice, sometimes at the middle of the recovery time, resulted from the surgery or from damage caused by battles between them resulting sometimes in necessary euthanizes.

It was necessary the antibiotic change for another one with larger spectrum.

During the experience it was also necessary made some protocol adjustments like the replacement of the OCT to paraffin for sample inclusion due to poor adhesion of sections of cryopreserved samples to slides. Bringing difficulties both during the handling of the sections in Eriochrome C/Cresyl violet staining, and then in the performance of the antibodies in immunofluorescence technique caused by the thickness of the OCT sections (30 µm). After change the inclusion medium and consequent slice thickness (6 µm), various protocols had to be adjusted, time consuming.

Conclusion

In our study at 2 weeks post trauma of the spinal cord, we observed a re-localization of HA expression in injured spinal cord. Despite HA degradation at the injury epicenter, where the bigger astrogliosis is present, any differences in overall HA amount were measured, suggesting that some regions within the cord down regulated HA expression while others up regulated HA synthesis. Corollary, we were not able to measure any statistical difference in the mRNA expression of HA metabolizing enzymes between uninjured and injured animals. In uninjured spinal tissue, we did not see any $GFAP^+$ cells nor $IBA1^+$ cells, what was expected given that these cells are quiescent in physiological conditions. However HA was detected by immunohistochemistry and immunofluorescence, suggesting that HA is present in the normal spinal cord and its turn-over very low. Using double immunohistochemistry, we observed a co-localization between HA and $GFAP^+$ or $IBA1^+$ cells in injured spinal cord, especially where HA is up regulated at the boundaries of the lesion core. Supplemental *in vitro* experiments should be carried out to confirm HA release by astrocytes or microglial cells after activation. If HA has the role to regulate astrocyte proliferation, we could, through the HA metabolizing enzymes regulation, activate and deactivate astrocytes proliferation, in the right time, and so promote or inhibiting HA synthesis, regulating the HA size and amount in lesion epicenter needed to promote axonal regeneration.

Finally the hypothesis formulated is that the HA accumulation in injury is located around lesion, as a shell, preventing the access of neural stem cells and consequent differentiation, to the injury site. Intriguingly, at two weeks after injury, we did not see any HA in the lesion core (only around). This finding deserves further investigations to help deciphering if this lack of HA does not contribute to the poor ability of the lesion core to re-permeate.

References

Alovskaya A., Alekseeva T., Phillips J. B., King V. and Brown R. (2011). **"Fibronectin, Collagen, Fibrin - Components of Extracellular Matrix for Nerve regeneration**." *Review Acta Neurobiology Experimental* **71**: 281–299.

Bickenbach J., Sorensen F. B., Knott J., Shakespeare T., Stucki J., Tharion G., Wee J. (2011). **"International perspectives on spinal cord injury."** *WHO Library Cataloguing* 3-10.

Basso D. M., Fisher L. C., Anderson A. J., Jakeman L. B., McTigue D. M., Popovich P. G. (2006). **"Basso Mouse Scale for locomotion detects differences in recovery after spinal cord injury in five common mouse strains."** *Journal of Neurotrauma* **23**: 635–659.

Berg V. M. E. L., Castellote J. M., Fernandez I. M., Cuesta J. P. (2010). **"Incidence of spinal cord injury worldwide: a systematic review."** *Neuroepidemiology* **34**: 184–192.

Boulland J. L., Lambert F. M., Züchner M., Ström S., Glover J. C. (2013). **"A Neonatal Mouse Spinal Cord Injury Model for Assessing Post-Injury Adaptive Plasticity and Human Stem Cell Integration."** *PLOS ONE* **8**: 1-19.

Bracken M. B. (2012). **"Steroids for acute spinal cord injury."** *Cochrane Database of Systematic Reviews* **18**: 1-6.

Burnside E. R. and Bradbury E. J. (2014). **"Manipulating the extracellular matrix and its role in brain and spinal cord plasticity and repair."** *Neuropathology Applied Neurobiology* **40**: 26–59.

Cafferty W. B. J., Yang S.H., Duffy P. J., Li S. and Strittmatter S. M. (2007). **"Functional Axonal Regeneration through Astrocytic Scar Genetically Modified to Digest Chondroitin Sulfate Proteoglycans."** *Journal of Neuroscience* **27**: 2176–2185.

Cyphert J. M., Trempus C. S. and Garantziotis S. (2015). **"Size Matters: Molecular Weight Specificity of Hyaluronan Effects in Cell Biology."** *International Journal of Cell Biology* **2015**:1-8.

De Jonge H. J. M., Fehrmann R. S. N., de Bont E. S. J. M., Hofstra R. M. W., Gerbens F., Kamps W. A.,. de Vries E. G. E, van der Zee A. G. J., te Meerman G. J., ter Elst A. (2007). "**Evidence Based Selection of Housekeeping Genes."** *PLoS ONE* **2**: 1-5.

Dicker K. T., Gurski L. A., Bhatt S. P., Witt R. L., Farach-Carson M. C., Jia X. (2014). **"Hyaluronan: A simple polysaccharide with diverse biological functions."** *Acta Biomaterialia* **10**: 1558–1570.

Dzwonek J. and Wilczynski G.M. (2015). **"CD44: molecular interactions, signaling and functions in the nervous system."** *Frontiers in Cellular Neuroscience* **9**: 1-8.

Faulkner J. R., Herrmann J. E., Woo M. J., Tansey K. E., Doan N. B. and Sofroniew M. V. (2004). "**Reactive astrocytes protect tissue and preserve function after spinal cord injury."** *The journal of Neuroscience* **24**: 2143-2155.

Fehlings M. G., Vaccaro A., Wilson J. R., Singh A., W Cadotte D, Harrop J. S., Aarabi B., Shaffrey

C., Dvorak M., Fisher C., Arnold P., Massicotte E. M., Lewis S., Rampersaud R. (2012). **"Early versus Delayed Decompression for Traumatic Cervical Spinal Cord Injury: Results of the Surgical Timing in Acute Spinal Cord Injury Study (STASCIS)."** *PLOS One* **7**: 1-8.

Gaudet A. D. and Popovich P. G. (2014). **"Extracellular matrix regulation of inflammation in the healthy and injured spinal cord."** *Experimental Neurology* **258**: 24–34.

Gupta D., Tator C. H., Shoichet M. S. (2006). **"Fast-gelling injectable blend of hyaluronan and methylcellulose for intrathecal, localized delivery to the injured spinal cord."** *Biomaterials* **27**: 2370–2379.

Harrison M., O'Brien A., Adams L., Cowin G., Ruitenberg M. J., Sengul G., Watson C. (2013). **"Vertebral landmarks for the identification of spinal cord segments in the mouse."** *Neuroimage* **68**: 22–29.

Jakeman L. B., Williams K. E. and Brautigam B. (2014). **"In the presence of danger: the extracellular matrix defensive response to central nervous system injury."** *Neural Regeneration Research* **9**: 377-384.

Khaing Z. Z., Milman B. D., Vanscoy J. E., Seidlits S. K., Grill R. J. and Schmidt C. E. (2011). **"High molecular weight hyaluronic acid limits astrocyte activation and scar formation after spinal cord injury."** *Journal of Neural Engineering* **8**: 1-12.

Koenig B., Pape D. , Chao O., BauerJ. and Grimpe B. (2015). **"Long term study of deoxyribozyme administration to XT-1 mRNA promotes corticospinal tract regeneration and improves behavioral outcome after spinal cord injury."** *Experimental Neurology (in press).*

Kundi S., Bicknell R. and Ahmed Z. (2013). *"**Spinal cord injury: current mammalian models.***" *American Journal of Neuroscience* **4**: 1-12.

Kwok J. C. F., Dick G., Wang D. and Fawcett J. W. (2011). **"Extracellular matrix and perineuronal nets in CNS repair."** *Developmental Neurobiology* **71**: 1073-1089.

Lau L. W., Cua R., Keough M. B., Haylock-Jacobs S. and Wee V. Y (2013). **"Pathophysiology of the brain extracellular matrix: a new target for remyelination."** *Reviews Neuroscience* **14**: 722–729.

Lee H., McKeon R. J. and Bellamkonda R. V. (2010). **"Sustained delivery of thermostabilized chABC enhances axonal sprouting and functional recovery after spinal cord injury."** Proceedings of the *National Academy* of Sciences of the United States of America **107**: 3340-3345.

Li K., Nicaise C., Sannie D., Hala T. J., Javed E., Parker J. L., Putatunda R., Regan K. A., Suain V., Brion J. P., Rhoderick F., Wright M. C., Poulsen D. J., Lepore A. C. (2014) **"Overexpression of the astrocyte glutamate transporter GLT1 exacerbates phrenic motor neuron degeneration, diaphragm compromise, and forelimb motor dysfunction following cervical contusion spinal cord injury."** *Journal of Neurosciences* **34**: 7622-7638.

Marques S. A., Garcez V. F., Del Bel E. A. and Martinez A. M. B (2009). **"A simple, inexpensive and easily reproducible model of spinal cord injury in mice: morphological and functional assessment."** *Journal of Neuroscience Methods* **177**: 183–193.

Moshayedi P., Carmichael S. T. (2013). **"Hyaluronan, neural stem cells and tissue reconstruction after acute ischemic stroke."** *Biomatter* **3**: 1-9.

Mothe A. J., TamR. Y., Zahir T., Tator C. H., Shoichet M. S. (2013). **"Repair of the injured spinal cord by transplantation of neural stem cells in a hyaluronan-based hydrogel."** *Biomaterials* **34**: 3775–3783.

Movaghar V. R., Sayyah M. K., Akbari H., Khorramirouz R., Rasouli M. R., Lakeh M. M., Shokraneh F., Vaccaro A. R. (2013). **"Epidemiology of traumatic spinal cord injury in developing countries: a systematic review."** *Neuroepidemiology* **41**: 65–85.

National Spinal Cord Injury Statistical Center, Facts and Figures at a Glance. Birmingham, AL: University of Alabama at Birmingham, February 2014.

New P. W. (2006). "**Non-traumatic spinal cord injury: what is the ideal setting for rehabilitation?"** *Australian Health Review* **30**: 353–361.

Nicaise C., Putatunda R., Hala T., Regan K., Frank D. M., Brion J. P., Leroy K., Pochet R., Wright M. C. and Lepore A. C. (2012). **"Degeneration of Phrenic Motor Neurons Induces Long-Term Diaphragm Deficits following Mid-Cervical Spinal Contusion in Mice."** *Journal of Neurotrauma* **29**: 2748–2760.

Oyinbo C. A. (2011). **"Secondary injury mechanisms in traumatic spinal cord injury: a nugget of this multiply cascade."** *Acta Neurobiologiae Experimentalis* **71**: 281–299.

Papakonstantinou E., Roth M., Karakiulakis G. (2012).**"Hyaluronic acid: A key molecule in skin aging."** *Dermato-endocrinology* **4**: 253-258.

Rowland J. W., Hawryluk G. W. J., Kwon B., Fehlings M.G. (2008). **"Current Status of Acute Spinal Cord Injury Pathophysiology and Emerging Therapies: Promise on the Horizon."** *Neurosurgurgical Focus* **25**: 1-17.

Sharma K., Selzer M. E. and Li S. (2012). **"Scar-mediated inhibition and CSPG receptors in the CNS."** *Experimental Neurology* **237**: 370–378.

Sherman L. S. and Back S. (2008). **"A 'GAG' reflex prevents repair of the damaged CNS."** *Trends in Neurosciences* **31**: 44–52.

Sherman L. S., Matsumoto S., Su W., Srivastava T. and Back S. A. (2015). **"Hyaluronan Synthesis, Catabolism, and Signaling in Neurodegenerative Diseases."** *International Journal of Cell Biology* **2015**: 1-10.

Silver J. and Miller J. H. (2004). **"Regeneration beyond the glial scar."** *Nature Reviews Neuroscience* **5**: 146-156.

Slevin M., Krupinski J., Gaffney J., Matou S., West D., Delisser H., Savani R. C. and Kumar S. (2007). **"Hyaluronan-mediated angiogenesis in vascular disease: uncovering RHAMM and CD44 receptor signaling pathways."** *Matrix Biology* **26**: 58–68.

Sloane J. A., Batt C., Ma Y., Harris Z. M., Trapp B., Vartanian T. (2010). **"Hyaluronan blocks**

oligodendrocyte progenitor maturation and remyelination through TLR2." *Proceedings of the National Academy of Sciences* **107**: 11555-11560.

Soleman S., Filippov M. A. , Dityatev A., Fawcett J. W. (2013). **"Targeting the neural extracellular matrix in neurological disorders."** *Neuroscience* **253**: 194–213.

Struve J., Maher P. C., Li Y.Q., Kinney S., Fehlings M.G., Kuntz C. and Sherman L. S. (2005). **"Disruption of the hyaluronan-based extracellular matrix in spinal cord promotes astrocyte proliferation."** *Glia* **52**: 16–24.

Suberviola B., González-Castro A., Liorca J, Ortiz-Melon F., MIÑAMBRES E. (2008). **"Early complications of high-dose methylprednisolone in acute spinal cord injury patients."** *Injury* 39: 748–752.

Tachi Y., Okuda T., Kawahara N., Kato N., Ishigaki Y. and Matsumoto T. (2015). **"Expression of Hyaluronidase-4 in a Rat Spinal Cord Hemisection Model."** *Asian Spine Journal* **9**: 7-13.

Taghva A, Hoh D. J., Lau C. L. (2012). **"Advances in the management of spinal cord and spinal column injuries."** *Handbook Clinical Neurology* **109**: 105–130.

Torigoe K. Tanaka H. F., Ohkochi H., Miyasaka M., Yamanokuchi H.,Yoshidad K. and Yoshida T. (2011). **"Hyaluronan tetrasaccharide promotes regeneration of peripheral nerve: in vivo analysis by film model method."** *Brain Research* **1385**: 85-92.

Yuan Y.M. and He C. (2013). **"The glial scar in spinal cord injury and repair."** *Neuroscience Bulletin* **29**: 421–435.

Wang J., Wang X., Rong W., Lv J., Wei F., Liu Z. (2014). **"Alteration in chondroitin sulfate proteoglycan expression at the epicenter of spinal cord is associated with the loss of behavioral function in Tiptoe walking Yoshimura mice."** Neurochemical Research **39**: 2394-2406.

Wang J., Rong W., Hu X., Liu X., Jiang L., Ma Y., Dang G., Liu Z. and Wei F. (2012). **"Hyaluronan tetrasaccharide in the cerebrospinal fluid is associated with self-repair of rats after chronic spinal cord compression."** Neuroscience **210**: 467-80.

Wang J., Wang X., Wei J. and Wang M. (2015). **"Hyaluronan tetrasaccharide exerts neuroprotective effect and promotes functional recovery after acute spinal cord injury in rats."** *Neurochemical Research* **40**: 98–108.

Wakao N., Imagama S., Zhang H., Tauchi R., Muramoto A., Natori T., Takeshita S., Ishiguro N., Matsuyama Y., Kadomatsu K. (2011). **"Hyaluronan oligosaccharides promote functional recovery after spinal cord injury in rats."** *Neuroscience Letters* **488**: 299–304.

Winkler C. W., Foster S. C., Itakura A., Matsumoto S. G., Asari A., McCarty O. J. and Sherman L. S. (2013). **"Hyaluronan oligosaccharides perturb lymphocyte slow rolling on brain vascular endothelial cells: Implications for inflammatory demyelinating disease."** *Matrix Biology* **32**: 160–168.

Yang C., Cao M., Liu H., He Y., Xu J., Du Y., Liu Y., Wang W., Cui L., Hu J. and Gao F.(2012). **"The High and Low Molecular Weight Forms of Hyaluronan Have Distinct Effects on CD44 Clustering."** *The Journal of biological chemistry* **287**: 43094 –43107.

Yuan Y. M. and He C. (2013). **"The glial scar in spinal cord injury and repair."** *Neuroscience Bulletins* **29**: 421-435.

Zhou X., He X. and Ren Y. (2014). **"Function of microglia and macrophages in secondary damage after spinal cord injury."** *Neural Regeneration Research* **9**: 1787-1795.

Web references

Alexander Edmond (1995-2015). Acceded in: 13/August/2015 in http://www.shannonassociates.com/artist/edmondalexander/category/21#url=3184.

Onken Michael (2001). What is hyaluronic acid?. Acceded in 17/August/2015 in http://www.madsci.org/posts/archives/2001-04/986571103.Bc.r.html.

https://www.nscisc.uab.edu. Acceded in 21/August/2015.